EFFECTS OF BORON COMPOUNDS ON THERMAL DEGRADATION
BEHAVIOUR OF POLYMERS INVOLVING ESTER LINKAGES

A THESIS SUBMITTED TO
THE GRADUATE SCHOOL OF NATURAL AND APPLIED SCIENCES
OF
MIDDLE EAST TECHNICAL UNIVERSITY

BY

NEZAKET NEHİR ÇETİNKAYA

IN PARTIAL FULFILLMENT OF THE REQUIREMENTS
FOR
THE DEGREE OF DOCTOR OF PHILOSOPHY
IN
POLYMER SCIENCE AND TECHNOLOGY

FEBRUARY 2021

Approval of the thesis:

EFFECTS OF BORON COMPOUNDS ON THERMAL DEGRADATION BEHAVIOUR OF POLYMERS INVOLVING ESTER LINKAGES

submitted by **NEZAKET NEHİR ÇETİNKAYA** in partial fulfillment of the requirements for the degree of **Doctor of Philosophy** in **Polimer Science and Technology, Middle East Technical University** by,

Prof. Dr. Halil Kalıpçılar
Dean, Graduate School of **Natural and Applied Sciences** _____

Prof. Dr. Necati Özkan
Head of the Department, **Polymer Science and Technology** _____

Prof. Dr. Jale Hacaloğlu
Supervisor, **Chemistry, METU** _____

Prof. Dr. Cevdet Kaynak
Co-Supervisor, **Metallurgical and Materials Eng, METU** _____

Examining Committee Members:

Prof. Dr. Necati Özkan
Polymer Science and Technology, METU _____

Prof. Dr. Jale Hacaloğlu
Chemistry, METU _____

Prof. Dr. Menemşe Gümüşderelioğlu
Chemical Engineering, Hacettepe University _____

Prof. Dr. Nursel Dilsiz
Chemical Engineering, Gazi University _____

Prof. Dr. Ali Çırpan
Chemistry, METU _____

Date: 10.02.2021

I hereby declare that all information in this document has been obtained and presented in accordance with academic rules and ethical conduct. I also declare that, as required by these rules and conduct, I have fully cited and referenced all material and results that are not original to this work.

Name Last name : Nezaket Nehir Çetinkaya

Signature :

ABSTRACT

EFFECTS OF BORON COMPOUNDS ON THERMAL DEGRADATION BEHAVIOUR OF POLYMERS INVOLVING ESTER LINKAGES

Çetinkaya, Nezaket Nehir
Doctor of Philosophy, Polimer Science and Technology
Supervisor : Prof. Dr. Jale Hacaloğlu
Co-Supervisor: Prof. Dr. Cevdet Kaynak

February 2021, 90 pages

Interest in polymer nanocomposites is growing exponentially across various scientific and engineering disciplines owing to their remarkable improvements in their properties compared to micro- and macro- conventional composites. Although polymers having good physical properties are commercially available, they are mostly hampered by their low melting temperatures, poor mechanical or barrier properties. Therefore, there is a considerable work on improvement of the properties of polymers, and development of polymer nanocomposites.

Several studies were concentrated on boron compounds in polymer composites in order to enhance thermal properties of polymers. Trans-esterification and/or condensation reactions between the boron compounds and the polymers involving COO, OH or CONH groups may take place and support to improve thermal characteristics. Boronic acid groups release water upon thermolysis and behave like condensed phase flame retardants and lead to the generation of boronic anhydrides and boroxines. They form a cross linked-boroxine network through water loss by assisting intermolecular interactions and so they are good char-yielding compounds.

In this study, composites of polymers having ester group along the main change such as poly(lactic acid), PLA and poly(caprolactone), PCL, or along the side chain such as poly(methyl methacrylate), PMMA and poly(n-butyl methacrylate), PnBMA with methyl tallow bis-2-hydroxyethyl ammonium modified montmorillonite, Cloisite 30B (C30B) and Cloisite 15A (C15A) and boron compounds (benzene-1,4-diboronic acid (BDBA), boric acid (BA) and zinc borate (ZB)) were prepared and characterized with the use of transmission electron microscopy (TEM) and x-ray diffraction (XRD) analyses. Dispersion of clay in the polymer matrices and intercalated and partially exfoliated clay layers were analyzed by both techniques.

Thermal characteristics of the nanocomposites were investigated by direct pyrolysis mass spectrometry (DP-MS) and thermal gravimetric analysis (TGA) techniques. The increase in thermal stabilities of PLA and PMMA were associated with generation of a crosslinked structure. On the other hand, the decrease in thermal stability of PCL upon incorporation of BDBA and/or C30B was attributed to lower probability of crosslinking in the presence of long alkyl chains along the polymer backbone. Generation of boron network structure was detected for PMMA-BDBA and PCL-BDBA composites.

For PnBMA, although addition of C30B increased the thermal stability, addition of clay with BDBA caused any noticeable change in thermal stability.

Trans-esterification reactions between BDBA and C30B and ester groups of polymer matrices were also determined.

Keywords: Polyesters, Polymer Composites, Electrospun Fibers

ÖZ

BORON BİLEŞİKLERİNİN, ESTER BAĞI İÇEREN POLİMERLERİN ISIL BOZUNUM DAVRANIŞLARI ÜZERİNDEKİ ETKİLERİ

Çetinkaya, Nezaket Nehir
Doktora, Polimer Bilim ve Teknolojisi
Tez Yöneticisi: Prof. Dr. Jale Hacaloğlu
Ortak Tez Yöneticisi: Prof. Dr. Cevdet Kaynak

Şubat 2021, 90 sayfa

Pek çok bilimsel ve mühendislik alanının, polimer nanokompozitlere karşı katlanarak artan ilgisinin sebebi, bu kompozitlerin bilinen mikro- ve makro-kompozitleri ile karşılaştırıldığında, özelliklerinde elde edilebilen dikkat çekici iyileşmelerdir. Polimerler, oldukça iyi fiziksel özelliklerine ve piyasada kolay ulaşılabilir olmalarına rağmen, çoğunlukla düşük erime sıcaklıkları, zayıf mekanik ya da bariyer özellikleri nedeniyle kısıtlı kulanım alanı bulmaktadır. Buna bağlı olarak, polimerlerin özelliklerinin iyileştirilmesine ve polimer nanokompozitlerin geliştirilmesine büyük çaba harcanmaktadır.

Pek çok çalışma, polimerlerin, ısıl karakteristiklerinin iyileştirilmesinde, polimer matrikslerine, boron bileşiklerinin eklenmesi üzerine yoğunlaşmıştır. Boron bileşikleri ile polimer zincirinde yer alan OH, COO ve CONH grupları arasında gerçekleşebilecek kondenzasyon ve/veya trans-esterifikasyon reaksiyonları, ısıl özelliklerin iyileşmesini sağlayabilir. Alev geciktiriciler gibi düşünülen boronik asit grupları, termoliz sırasında su çıkararak, boroksin ya da boronik anhidrat oluşumuna neden olmaktadır. Boronik asitlerin, yoğun fazda moleküller arası etkileşimlere yardımcı olarak, su kaybıyla, çapraz bağlı boroksin ağı oluşturduğu gösterilmiştir.

Bu çalışmada, poli(laktik asit), PLA ve poli(kaprolakton), PCL gibi ana zincirinde, ya da poli(metil metakrilat), PMMA ve poli(n-bütil metakrilat), PnBMA gibi yan zincirinde ester grubu içeren metil (tallow) bis-2-hidroksietil amonyum modifiyeli montmorillonit, Cloisite 30B (C30B)`li ve Cloisite 15A (C15A)`lı polimerlerin, boron bileşikleri ile (benzen-1,4-diboronik asit (BDBA), borik asit (BA) ve çinko borat (ZB) ile kompozitleri hazırlanmış ve karaterize edilmiştir. Boron bileşik miktarının, morfoloji üzerine etkisi sistematik olarak geçirimli electron mikroskopu (TEM) ve x-ışını difraksiyonu (XRD) analizleri ile araştırılmıştır. Her iki tekniğin sonuçlarına göre, kil yapılarının polimer matrisleri içinde dağıldığı ve katmanlarının aralarının açıldığı ve kısmen ayrıldığı saptanmıştır.

Kompozitlerin ısıl davranışları, direkt piroliz kütle spektrometre, termogravimetre ve diferansiyel termal analiz yöntemleri kullanılarak açıklanmıştır. BDBA ve C30B eklendiğinde, PLA ve PMMA'nın ısıl özellikleri, çapraz bağlı yapıların oluşumuyla artarken, PCL'nin ısıl kararlılığı, muhtemelen polimer omurgasındaki uzun alkil zincirin, çapraz bağ olasılığını azaltmasından kaynaklı olarak düştüğü gözlenmiştir.

PnBMA için ise, C30B eklenmesi ısıl kararlılığı arttırırken, kilin BDBA ile birlikte kullanılması, ısıl kararlılıkta fark edilir bir değişime neden olmamıştır.

BDBA, C30B ve polimerlerdeki ester grupları arasında trans-esterifikasyon reaksiyonları tespit edilmiştir.

Anahtar Kelimeler: Poliesterler, Polimer Kompozitler, Elektroeğirme Lifler

To memory of my dad

ACKNOWLEDGMENTS

TABLE OF CONTENTS

LIST OF TABLES

LIST OF SCHEMES

LIST OF FIGURES

FIGURES

xvii

LIST OF ABBREVIATIONS

ABBREVIATIONS

BA	Boric acid
BDBA	Benzene-1,4-diboronic acid
C15A	Cloisite 15A
C30B	Cloisite 30B
CTEM	Conventional transmission electron microscopy
DCM	Dichloromethane
DMF	Dimethylformamide
DPMS	Direct pyrolysis mass spectrometry
DTG	Differential thermal gravimetry
GC	Gas chromatography
MMT	Montmorillonite
M_n	Number average molecular weight
M_w	Weight average molecular weight
PCL	Poly(ε-caprolactone)
PI	Polydispersity index
PLA	Poly(lactic acid)
PMMA	Poly(methyl methacrylate)
PNBMA	Poly(n-butyl methacrylate)
SEM	Scanning electron microscopy
STA	Simultaneous thermal Analysis
TEM	Transmission electron microscopy
T_g	Glass transition temperature
TGA	Thermal gravimetric analysis
TIC	Total ion current
T_m	Melting temperature
T_{max}	Maximum degradation temperature
XRD	X-ray diffractometer
ZB	Zinc borate

CHAPTER 1

INTRODUCTION

1.1   Polymer Composites

Composite materials are multi-phase structures consisting of a matrix and reinforcing fillers that are integrated with the matrix, commonly resulting in synergistic properties that cannot be achieved from matrix material alone[1-3]. The composite materials are classified according to their matrix such as: metallic, ceramic and polymer composites. Polymer composites are one of the most promising materials due to their low density, easy processability and commercially availability. However, their low melting temperatures and poor thermal or mechanical properties mostly hamper their applications. Therefore, polymer composites combining the advantages of the reinforcing materials (e.g. thermal stability, rigidity and stiffness) and organic polymers (e.g. processability, flexibility and ductility) have been extensively studied during the last decade [2-4] . Furthermore, if at least one dimension of the reinforcement material in the composite is in nanometer scale, much stronger and stiffer materials called nanocomposites can be obtained compared to micron scale composites as less defected structures can be prepared due to the elimination of secondary bonds. Nanomaterials have large external areas due to their small size. Ultra-large interfacial area density between the nanomaterial and the polymer can be obtained by uniform dispersion of these nanomaterials in a polymer matrix. Remarkable improvements in specific properties of the polymers are achieved even if nanostructured materials are added in low amounts (typically, less than 5 wt. %). Mechanical properties [5-6], thermal stability [7-8], gas barrier properties[9], electric properties[10] and even biodegradation rates[11-12] are commonly observed enhancements. Therefore, polymer nanocomposites are becoming a remarkable

branch by the introduction of nanoscale reinforcement materials into the polymer matrices in order to improve the properties of polymers compared to the neat polymer and micro- or macro- composites [13].

1.2   Polymer Matrices: Polymers Involving Ester Linkages

Matrix is the continuous and generally the softer part of a composite system. In the previous works in our research group, it was shown that some specific reactions may take place between OH, COO or CONH group along the polymer chain and the boron compounds[14-15]. Consequently, for the preparation of the composite materials, different types of polyesters were chosen in this study. The main difference between the selected polyesters was the position of the ester group in the structures. The ester groups are located along the main change for and poly(caprolactone), PCL and poly(lactic acid), PLA, whereas, they are along the side chain for poly(methyl methacrylate), PMMA and poly(n-butyl methacrylate), PnBMA.

1.2.1   Poly(ε-caprolactone)

Poly(ε-caprolactone) is a linear, aliphatic, semi-crystalline polyester. Figure 1.1 shows the chemical structure of PCL.
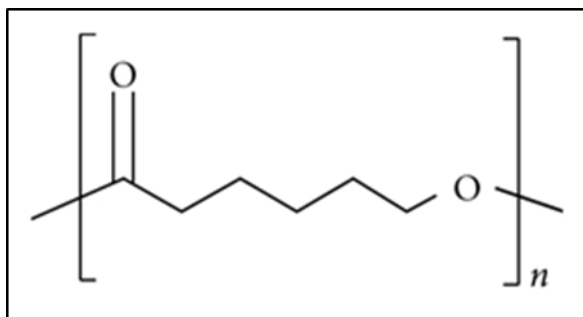
Figure 1. 1. Structure of poly(ε-caprolactone)

It has potential applications in several areas such as food packaging[16], pharmaceutical controlled release[17-18] and tissue engineering[19] due to its biodegradability and biocompatibility [20]. PCL is a render polymer for various applications due to its outstanding properties contrary to its aliphatic polyester counterparts. It provides a promising tool to fabricate longer term degradable implants having tailorable degradation kinetics to suit a specific anatomical site [21]. Although PCL is biodegradable and renewable, its industrial use is limited due to its poor mechanical and barrier properties because of its relatively low T_g and T_m values and thus its inherent shortcomings may be overcome by nanocomposite technology [22].

1.2.2   Poly(lactic acid)

Compared with the other biodegradable polymers, Poly(lactic acid), PLA, is a mostly studied polymer due to its properties like compatibility, transparency, high strength and modulus. In addition, it is called as `green` polymer due to its producibility from starch and corn that makes it biodegradable. Figure 1.2 shows the chemical structure of PLA.
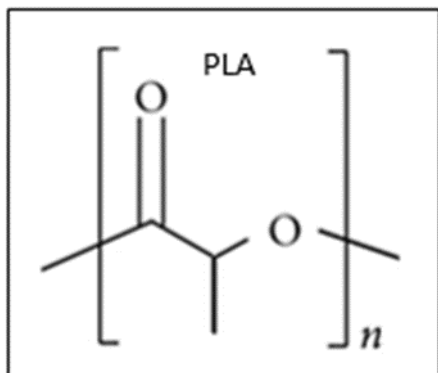
Figure 1. 2. Structure of poly(lactic acid)

PLA based nanocomposites with nanofillers as annexing agent have shown to have great potential especially in biomedical field [23]. Properties of PLA nanocomposites can be improved with the help of surface effect and small scale of nanomaterials compared to pure PLA materials in synthetic bone substitute and repair, tissue engineering, and drug delivery system.

Nanocomposites with PLA or PLA copolymers as matrix significantly help to overcome its shortcomings. Several studies have been performed in the last decades using some fillers like clay minerals, carbon nanotubes and graphene and its precursor to obtain nanocomposite materials [24].

1.2.3 Poly(methyl methacrylate)

Poly(methyl methacrylate) (PMMA) is a transparent polymer having chemical, weathering, and corrosion resistance properties [25]. PMMA has been used in sensors, electronic devices, drug delivery, coatings, additives and biomedical appliances [26-27]. Figure 1.3 shows the chemical structure of PMMA.
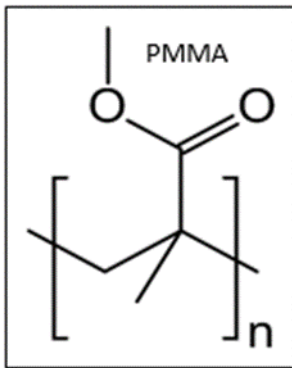
Figure 1. 3. Structure of poly(methyl methacrylate)

However, PMMA does not have appropriate thermal stability and mechanical properties for high-tech applications. Thus, in order to improve the performance of

this polymer, different nanomaterials have been used as nanofillers. PMMA plays an important role in the field of nanocomposite due to its fine compatibility and processability with different nanofillers [28-29].

1.2.4 Poly(n-butyl methacrylate)

Poly(n-butyl methacrylate), PnBMA is usually used in coatings, biomedical materials such as bone cement [30] and controlled release drug delivery systems [31]. Because its glass transition temperature is low and mechanical properties are relatively poor, PnBMA is more often as a modifier in polymer blends to obtain appropriate properties for various purposes. In order to improve these properties, inorganic fillers are often combined with PnBMA to form reinforced composites [30]. Figure 1.4 shows the chemical structure of PnBMA.
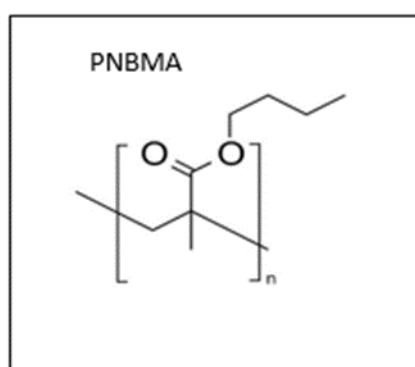
Figure 1. 4. Structure of poly(butyl methacrylate)

1.3 Reinforcement Materials

The reinforcement materials play important roles in controlling the properties of the composite structures. In this study, considering the results of the previous works of our research group[14-15] and the literature, two different reinforcing materials; different boron compounds, benzene-1,4-diboronic acid, boric acid and zinc borate

that may cause some specific reactions with the ester groups of the polymer chains and different nanoclays or methyl tallow bis-2-hydroxyethyl ammonium modified montmorillonites such as Cloisite 30B and Cloisite 15A were used.

1.3.1   Boron Compounds

Boron compounds are generally used as flame retardants. Contrary to halogenated flame retardants which produce toxic gases under burning, boric acid, zinc borate and boron oxide are non-toxic and environmentally friendly. Additionally, by lowering the heat flow, they can also restrict further pyrolysis of the polymers. One of these compounds, boronic acid produces water molecules during thermolysis process and forms boraxine or boronic acid anhydride. Boraxine glass structure may be produced by the water elimination at high temperatures when if more than one boronic acid functional group exists. Generation of char layer on the polymer surface which prevents the oxidation of carbon by limiting the accessible oxygen is occurred due to the glassy network. One of the examples of boronic acids is benzene-1,4-diboronic acid and its glassy network structure were shown in Figure 1.5.
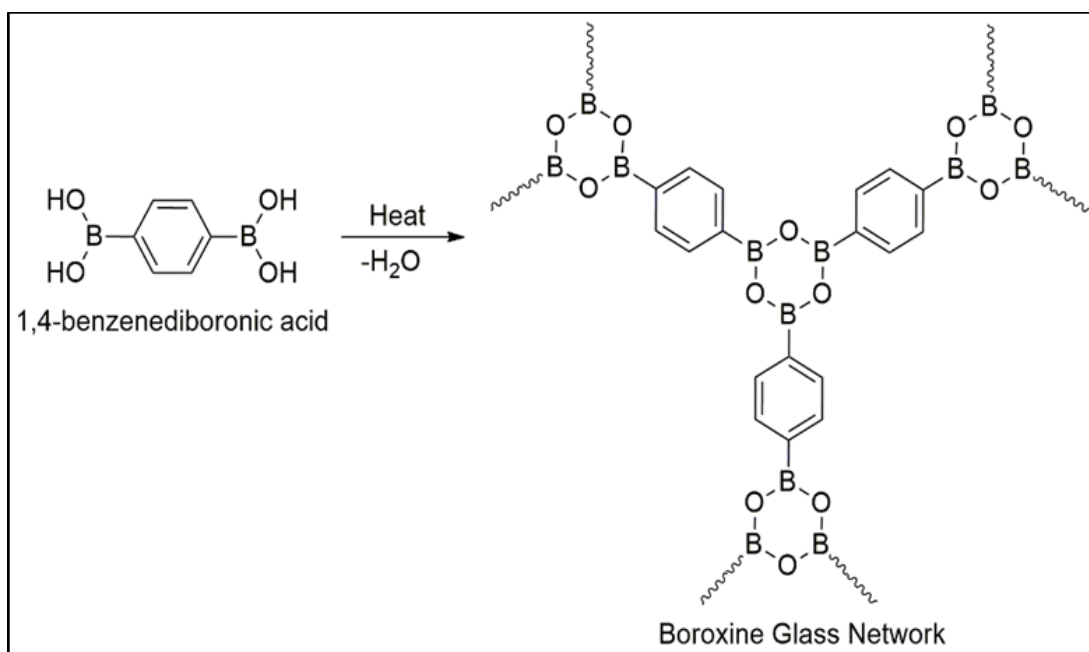
Figure 1. 5. Structure and glassy network formation of benzene-1,4-diboronic acid

Trans-esterification reaction is also possible between hydroxyl groups of boronic acid and alkoxy groups producing boronic ester structure. The effect of boronic acid on thermal and flame retardant properties is chemically by crosslink formation as well as physically by char layer construction.

Previous studies of our research group showed that increase in the amount of boron compounds reacting with polyesters enhance the intercalation and increase thermal stabilities of the polymers[14-15]. Therefore, the use of BDBA as a reinforcement material was also preferred in this study.

1.3.2   Nanoclays (Montmorillonites, MMT)

Montmorillonite (MMT) is a 2D, layered reinforcement material which is obtained from natural clay, bentonite. It has 2:1 layered silicate structure: Two tetrahedral silicate layer sandwiching a central octahedral alumina layer. The structure of MMT is given in Figure 1.6.
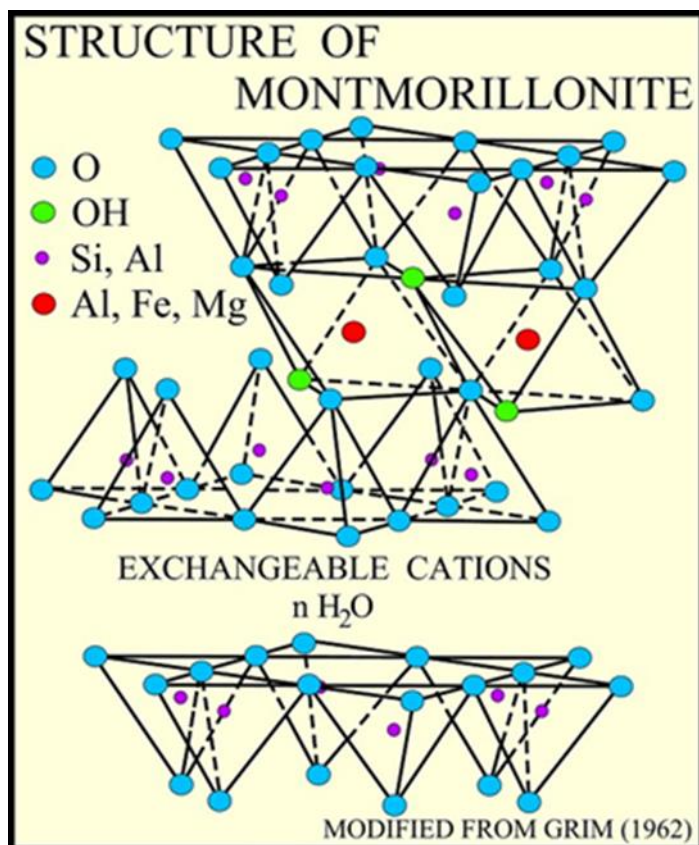
Figure 1. 6. Structure of montmorillonite

Among the different types of nanofillers, those based on layered silicates or clays, especially natural MMT, have been most widely investigated [32]. Indeed, silica-based nanocomposite systems are really attractive especially in industrial fields because of their remarkable properties such as high modulus, high heat resistance, reducing gas permeability by retaining the flexibility and flammability, etc. of its nanocomposites [22]. Addition of nanoparticles, such as nanoclays with ultralarge interfacial area per volume with a larger interfacial region (sheet-like structure) along with proper organic modification to form nanocomposites has provided the means to improve materials performance [33].

1.4　Nanoclay-Polymer Interaction

There should be an optimum interfacial bond strength between matrix and the reinforcement because the load (thermal, mechanical, etc.) should be transferred from matrix to reinforcement. However, strong tendency to form aggregate formation due to different nature of the nanofiller (inorganic) with respect to polymer matrix (organic), good dispersion is not easy to achieve. The performance of composites depends on the degree of homogeneity achieved in the dispersion of the nanofiller into the host polymer[21]. With this aim, for nanoclays, some interfacial treatments can be performed such as purification, organic modification and compatibilization. Organic modification based on ion exchange is the most favorable approach in literature. In order to promote compatibility between polymer and the reinforcement, inorganic clay cations should be exchanged with organic ones and for this purpose, mostly, quaternary ammonium compounds are used [22]. In Figure 1.7 shows the ion exchange mechanism of organic modification.
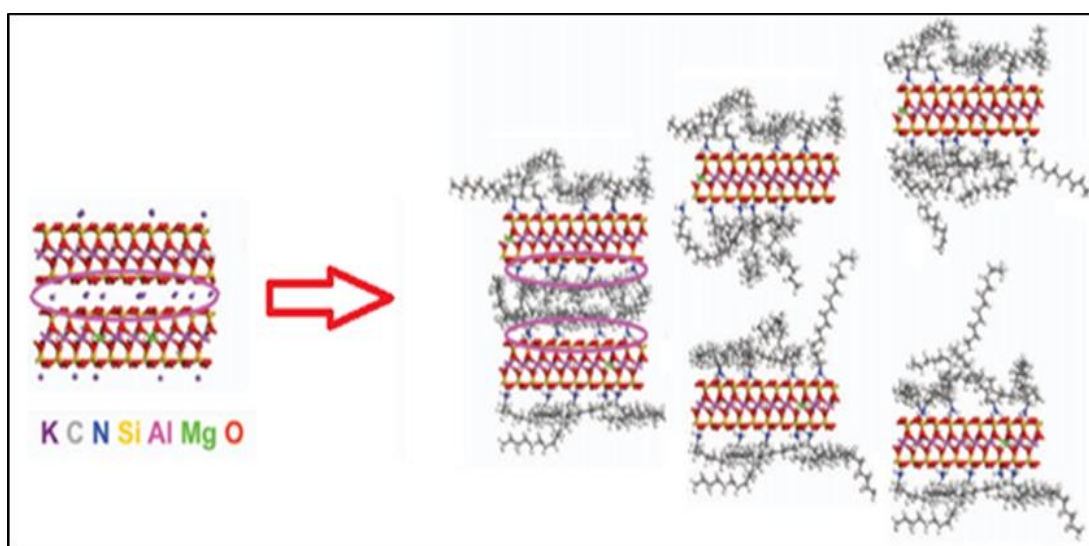
Figure 1. 7. Schematic representation of ion exchange mechanism

Two complementary mechanisms can be achieved by ion exchange with quaternary ammonium compounds. Firstly, since the polyesters are generally hydrophobic, hydrocarbon chains of these compounds increase the compatibility. Secondly, the interlayer distance between the clay layers increases with long alkyl chains present in these compounds that can also enter the space between the layers as shown in Figure 1.7.

Figure 1.8 represents the structures and names of some commercial organically modified montmorillonites.
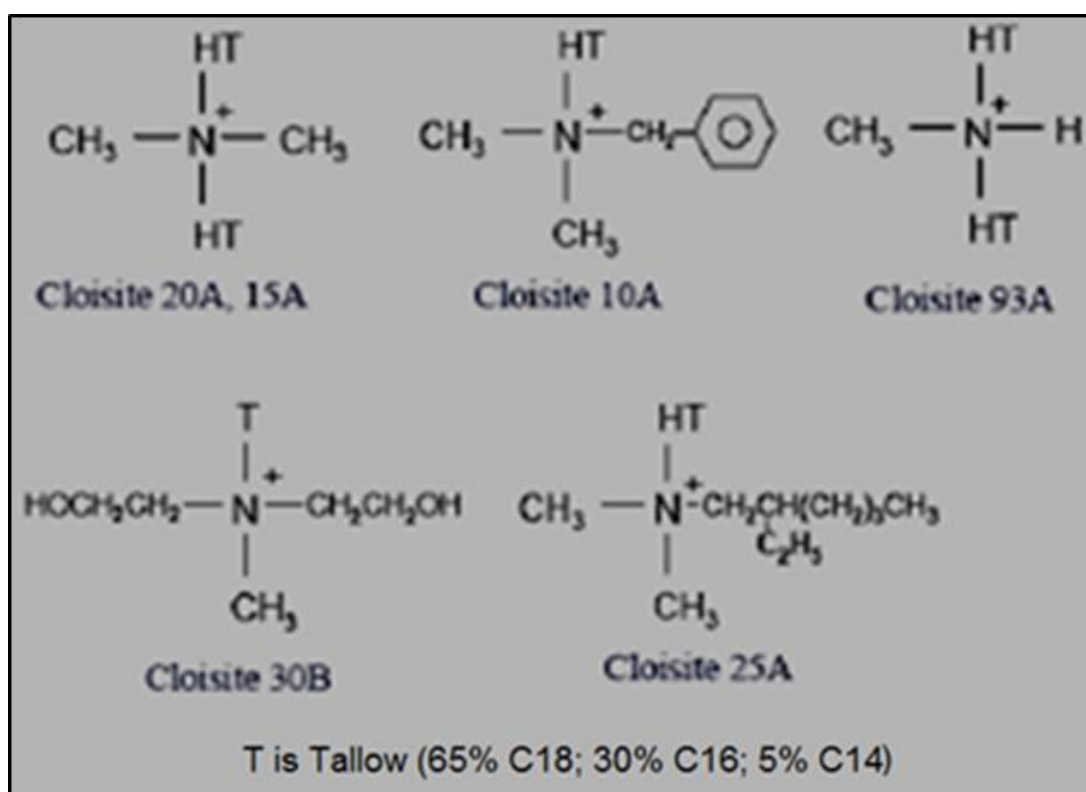
Figure 1. 8. Structures and commercial names of OMMTs

In this study, Cloisite 30B (C30B) and Cloisite 15A (C15A) were selected for the preparation of the clay reinforced composites.

1.5   Processing of Polymer Composites

Polymer nanocomposites can be prepared by three different mixing methods: Melt intercalation, solution intercalation and in-situ intercalation. In the melt mixing (intercalation for layered nanocomposites), solid polymer and surface treated nanoparticles (nanoclays) are mixed, melted, sheared and dispersed by using generally twin-screw extruder or internal mixer. Then the mixture is cooled either by using air or water. Melt mixing (intercalation) is the most industrial-friendly method that suitable for many thermoplastics. In solution mixing (intercalation), polymer and nanoparticles (nanoclays) are dissolved in a proper solvent by a mechanical mixer and then sheared by using a magnetic mixer and then dispersed with an ultrasonic mixer. The solution is placed into a vacuum oven to evaporate the solvent. Solution mixing (intercalation) is a useful technique for the thermoplastics that may degrade during melt mixing (i.e. conductive polymers). In the last method, in-situ polymerization (intercalation), monomers or oligomers are used and mixed with reinforcement material (nanoclays), initiator, crosslinking or curing agent depending on the type of polymer. Then polymerization takes place by shearing or dispersing. In the final step, curing or vulcanization is performed. This type of processing is important especially for thermoplastics and elastomers. Schematic representations of processing types are shown in Figure 1.9.
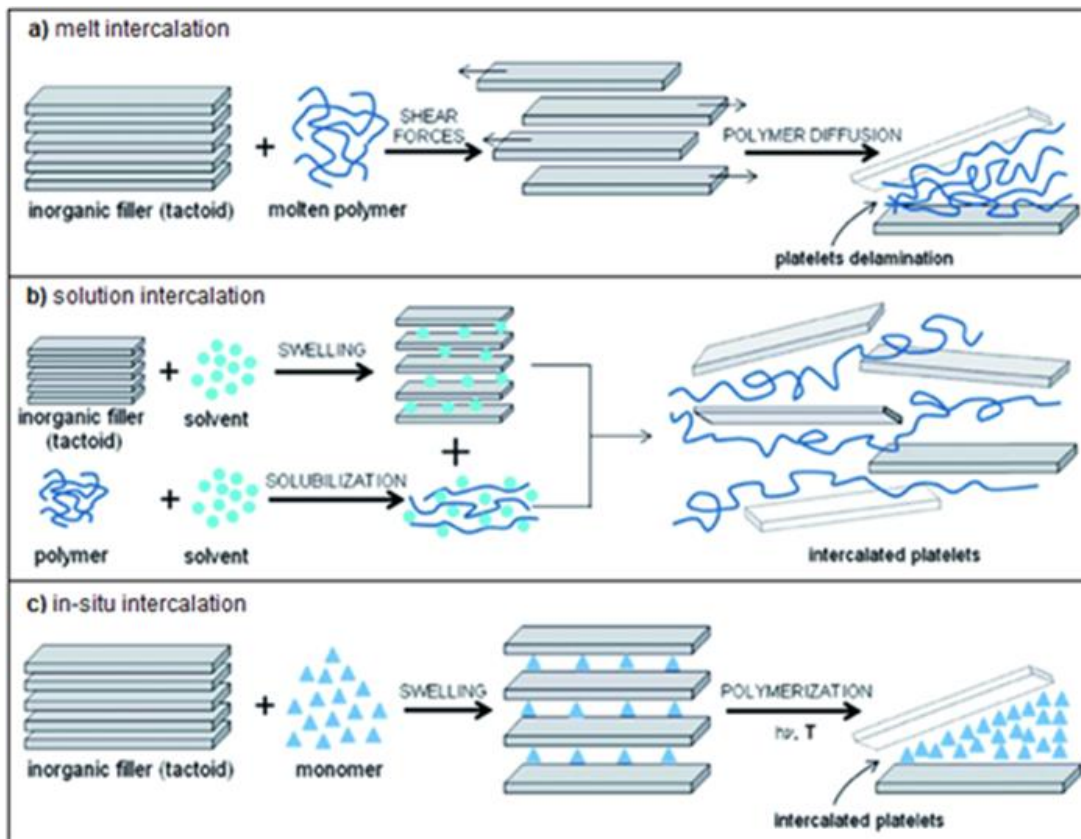
Figure 1. 9. Schematic representations of a) melt, b) solution and c) in-situ intercalation processes

In this study, all the composites were prepared by solution casting method. Chloroform was used as the solvent. All solid chemicals were stored in vacuum oven before usage. Solutions were stirred for two hours with a magnetic stirrer to obtained homogenous mixture.

1.6   Polymer Fibers

Electrospun polymer nanofibers are attracting growing interest due to their biocompatibility and biodegradability in particularly biomedical applications. Composite nanofibers can be considered as a good alternative for such applications by synergizing the preferred properties of multiple components. These

are mostly composed of a synthetic polymer and a distinct dispersed phase or phases consisting of inorganic or metal nanoparticles, drug nanocarriers, bioactive macromolecules, carbon nanostructures or natural polymer nanofibers. Composite nanofibers can be produced by surface modification of preformed nanofibers or by phase blending during electrospinning [31].

1.6.1   Electrospinning

For the production of polymer fibers, electrospinning is one of the most efficient way due to ranging of fiber diameters from several microns to tens of nanometers [35-37]. In order to induce charged polymer droplets, a high electrical field is used in the electrospinning process. With the help of electrical force, while the solution jet travels, it is elongated and whipped continuously accompanied by the evaporation of solvent. When they are deposited on the oppositely charged collector, the fibers are formed [38]. Figure 1.10 illustrates the production of electrospun fibers.
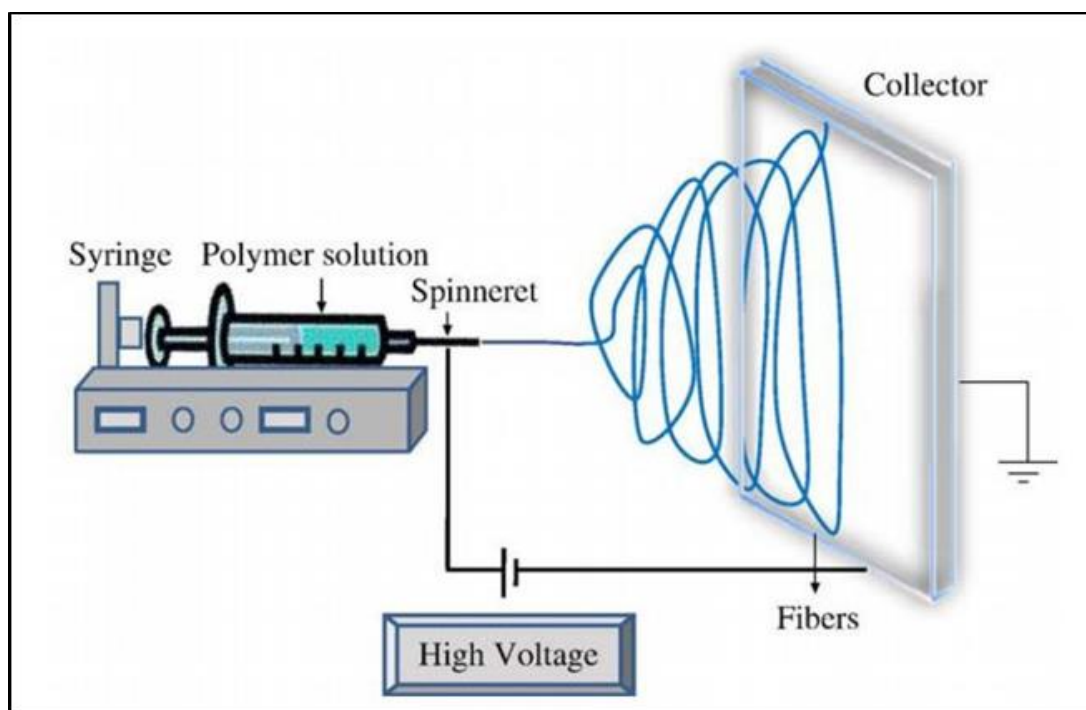
Figure 1. 10. Schematic representation of electrospinning process

Fibers having smooth surface and solid-core cross-section can be produced by electrospinning process. These fibers have been used in biosensors, tissue engineering, filtration or catalysis [39-40]. Additionally, the effect of properties of fibers can be improved by increasing surface area. Consequently, fibers having specific structures like hollow, porous surface or coresheath can offer many advantages for the applications such as drug delivery or tissue engineering scaffolds [41-42].

1.7   Literature Review of Polyester-Clay Composites

Dalir et al tried to prepare highly exfoliated polyester-clay nanocomposites and defined process-property correlations [43]. They used various amounts of three different types of clays, Cloisite 11B, Cloisite 15A and Cloisite 30B. Composites were prepared using solvent-based technique and used different mixing strategies.

Expansion properties were examined by dynamic mechanical thermal analyses for determining an optimized mixing strategy. They showed that coefficient of thermal expansion and glass transition temperatures slightly increased upon nanoclay addition. Moreover, they also determined that when higher amounts of esterificated nanoclay was added, coefficient of thermal expansion was decreased suggesting that nanoclays provide a restraining action and so increase in the extent of expansion of polyester network [43].

In another work, Bagheri et al prepared nanoclay (Cloisite 30B) and lead monoxide involving composites with unsaturated polyester matrix. They examined thermal resistance of the composites by thermogravimetry analyses. Thermal characteristics of composites was investigated by comparison of T_{dec} at specific weight loss. They showed that unsaturated polyesters involving C30B decomposed at slightly higher temperatures than neat unsaturated polyester. They explained this behavior with barrier effect of exfoliated clay layers for the heat transfer by hindrance of volatile decomposition products into the polymer matrix. Therefore, they proposed that addition of nanoclay may enhanced the thermal resistance of unsaturated polymers [44].

Romanzini et al focused on chemical modifications (silane-modified) of montmorillonite to improve MMT interaction with unsaturated polyester resin. They studied thermal properties of composites prepared using commercial C30B and C15A. Results showed that C30B and C15A had better dispersion and tendency to exfoliate compared to silane-modified clays causing delayed thermal volatilization of clay barrier effect [45].

In a similar study, Chieruzzi et al found reduced total heat of reaction for unsaturated polyester composites involving quaternary ammonium salt modified clay compared to neat resin. They suggested that intercalation of clay within resin prevents crosslinking which was confirmed by crosslinking density values [46].

Lepoittevin et al prepared PCL nanocomposites with natural (Cloisite-Na) and organically modified montmorillonites (Cloisite 30B and Cloisite 25A) and

investigated thermal behaviors by using thermogravimetry and differential scanning calorimetry techniques. Decomposition of clay involving composites shifted to higher temperatures compared to neat PCL. This behavior was associated with decrease in the extent of diffusion of oxygen and volatile products throughout the composite material. Moreover, they also observed that as the amount of clay added was increased decomposition temperature was decreased [47].

Early works in our group showed that use of clays and boron compounds as additives in polymer matrixes improved thermal characteristics of polymers. The improvements were mainly due to condensation and/or trans-esterification reactions between the boron compounds and OH, COO or CONH group present along the polymer chain [14,48].

In one of these studies, Akar prepared PLA composites involving different amounts of BDBA in the absence and the presence of C30B. TGA and DPMS results indicated that thermal stability increased especially with the increase in the amount of BDBA added. Although at low concentrations, decomposition temperature of PLA composites decreased, due to trans-esterification reactions between boron compound and polymer, generation of crosslinked structure occurred and thermal stability increased at high BDBA concentrations [14].

In another study, Ozdemir prepared and characterized PMMA composites involving different clays. She showed that thermal stability of the composites increased with the increase in the interlayer spacing of the silicate layers associating with better intercalation of polymer into the clay layers. Moreover, reactions between hydroxyl and amine groups of organic modifiers of clays and ester groups of polymers were detected pointing out generation of thermally more stable chains [48].

1.8 Aim of Work

In this work, different polyester composites involving two different types of clays (C30B and C15A) and three different boron compounds 1,4-benzenediboronic acid

(BDBA), boric acid (BA) and zinc borate (ZB) as improver were prepared. After solution casting, X-Ray Diffractometer and Transmittance Electron Microscopy analyses were performed in order to obtain morphological information of polymer-clay composites. Then thermal degradation behaviors of composites and their electrospun fibers were investigated with Direct Pyrolysis Mass Spectrometry and Thermal Degradation Analysis techniques. To characterize morphological properties of fibers, Scanning Electron Microscopy data were collected systematically.

CHAPTER 2

EXPERIMENTAL

2.1 Materials

PLA (M_n ~190000) and PCL (M_n ~45000) were purchased from Cargill Dow LLC and Sigma-Aldrich Co, respectively. PMMA (M_n ~105000) was provided by Sumitomo Chemical Co. Ldt. PnBMA (M_n ~1500, M_w ~1700, PI = 1.2) was received from Polymer Source. Methyl tallow bis-2-hydroxyethyl ammonium modified montmorillonite Cloisite 30B (C30B) and dimethyl dihyrogenated tallow quaternary ammonium modified montmorillonite Cloisite 15A (C15A) were acquired from Southern Clay Products Inc. Their cation exchange capacities are 90 meq/100g clay with 1.85 nm interlayer space between clay layers (d_{001}) and 125 meq/100g clay with 3.15 nm, respectively. Benzen-1,4-diboronic acid, BDBA (95.0% purity), boric acid, BA (99.5% purity) and zinc borate, ZB were purchased from Sigma-Aldrich Co. Solvents, chloroform, $CHCl_3$ (99%), dicholoromethane, DCM (99%) and dimethyl formamide, DMF (99%) were acquired from also Sigma-Aldrich Co. All materials were used as received without further purification.

2.2 Preparation Methods

2.2.1 Preparation of Polymer Composites

All the composites with various concentrations (3wt% for clays, 3%, 7% and 15wt% for boron compounds) were prepared by solution casting method. Chloroform was used as the solvent. All chemicals were stored in the vacuum oven before using. Solutions were stirred for two hours with a magnetic stirrer (1000 rph). Before XRD

and TGA analysis, solutions were poured onto Teflon surfaces and waited for all solvent evaporated.

2.2.2   Preparation of Electrospun Fibers

Solutions were spun with 1 ml syringes having metallic needles with 0.6 mm inner diameter in an enclosed chamber for the preparation of the fibers. New Era Pump Systems, Inc NE 300 was used and syringe was positioned horizontally. In the opposite of syringe with the 10 cm distance (tip to collector), a metal collector covered with aluminum foil was placed. Positive and negative electrodes of the voltage supply were clamped to both the metal collector and the needle. Flow rate of the polymer solutions was chosen 0.5 ml/hour and the 12.5 kV voltage was applied. Solvent systems and polymer solutions having various concentrations were attempted.

2.3   Characterization Techniques

2.3.1   Morphological Analyses

2.3.1.1   X-ray Diffractometer

Morphology of nanocomposites were mainly characterized by X-Ray Diffraction (XRD) technique. XRD has two important uses for the analysis of composites. It helps to determine the changes in the crystallinity of polymer matrix ($2\theta > 10°$) (e.g. changes in the amount and the type of the crystal phases, formation of new crystal phases) and the changes in the crystal structure of nano-reinforcement ($2\theta < 10°$) (e.g. level of interaction, exfoliation or distribution). Rigaku X-ray diffractometer, Miniflex with CuKα (30 kV, 15 mA, $\lambda = 1.54051$ Å) was used in order to analyze 2θ XRD patterns of the composites. The scanning range of the XRD patterns were 1° to 30°.

2.3.1.2   Transmission Electron Microscopy (TEM)

The internal structures of nanocomposites can be visualized via transmission electron microscopy (TEM). TEM allows a qualitative determination of the dispersion state (exfoliated / intercalated / microcomposite) of the reinforcement through direct visualization. Besides for a reliable qualitative evaluation, images should be taken with different magnifications from truly representative areas of the samples.

TEM analyses were performed by using a FEI Tecnai G2 Spirit Bio Twin CTEM. Nanocomposite solutions prepared in chloroform were poured into carbon coated-cupper grid (3 mm diameter and 400 mesh). Then the grids were allowed to dry in room temperature before the analyses.

2.3.1.3   Scanning Electron Microscopy (SEM)

Scanning electron microscopy (SEM) is also a useful tool for the characterization of composites especially for the analysis of morphology of the electrospun fibers. SEM images were examined with a FEI Nova NanoSEM 430 JSM 6400 Electron Microscope (JEOL). Before imaging, all samples were coated with 5nm Au/Pd (PECS-682).

2.3.2   Thermal Analyses

2.3.2.1   Simultaneous Thermal Analyses (STA)

Simultaneous thermal analyses gives information on the changes in the sample weight corresponding a temperature program comparing the sample with a reference as a function of time, simultaneously. In this work, a Perkin Elmer Simultaneous Thermal Analyzer 6000 was used. During the analysis, all the parameters were optimized constant flow rates were between 19.8 - 20 ml/min (under nitrogen

atmosphere) and the sample weights were approximately 8 mg in all experiments. Samples were hold at 100°C for 20 min in order to evaporate solvent and water that may be adsorbed. Then, they were cooled to 30°C and then finally, heated from 30°C to 550°C with a 10.0°C per minute heating rate.

2.3.2.2 Direct Pyrolysis Mass Spectrometer (DP-MS)

Direct pyrolysis mass spectrometry is a technique in which a material is degraded using a selected temperature program under high vacuum and consequently separated into its fragments. The products are ionized and separated according to m/z ratios and then analyzed. During the ionization process, some secondary reactions that may occur completely eliminated as the products of pyrolysis are removed immediately from the heating zone under high vacuum conditions. Surely, the pyrolysis fragments further dissociate during the ionization process and complicated mass spectrums are obtained. Therefore, generation of the degradation products should be analyzed in detail with the help of total ion current curves and single ion evolution profiles of the selected ions.

In this study, Waters Micromass Quattro Micro GC Mass Spectrometer was coupled to a direct insertion probe. All samples were heated from 50°C to 650°C with 10°C/min heating rate. Quartz vials were used. The scanning rate was 1 scan/s and the ionization energy was 70 eV. For all analyses, solution casted composites were prepared by dissolving 100 mg composite into 2 ml chloroform and placed in a vacuum oven at 60°C for one hour evaporate the solvent. The same amount of sample was analyzed in each experiment. All analyses were repeated at least twice to confirm the reproducibility.

CHAPTER 3

RESULTS AND DISCUSSIONS

3.1   Morphological Results

XRD patterns were recorded for polyesters, clays, boron compounds and composites in order to evaluate dispersion of clay and boron into polyester matrices. In order to support XRD analysis, TEM analysis were performed to visualize the clay layer separations.

3.1.1   XRD Patterns and TEM Images of PCL and Its Composites

XRD patterns were analyzed to determine the inter-layer spacing and the dispersion states of clay platelets. In Figure 3.1, X-ray diffractogram of C30B and BDBA composites with several ratios of PCL were given.
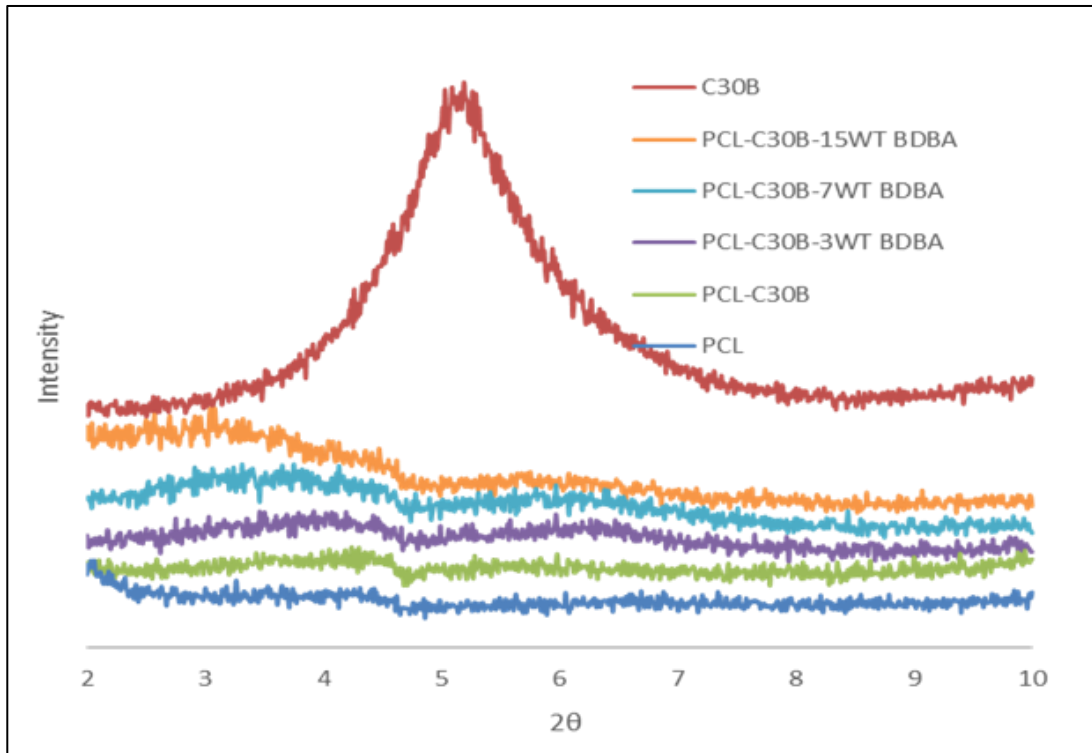
Figure 3. 1. X-ray diffractogram of C30B, PCL, PCL-C30B and PCL-C30B-BDBA composites

The C30B diffractogram has a characteristic peak at around $2\theta=5.0°$ corresponding to an inter-reticular distance of $d_{001}=1.8$ nm. This distinct peak was almost disappeared for all composites of PCL. Disappearance of the peak can be considered as both dispersion of clay structures into the polymer matrix and the well separation of the tactoid structure of clays. In order to support this inference, TEM images of PCL-C30B-BDBA composites with different boron amounts were represented in Figure 3.2.
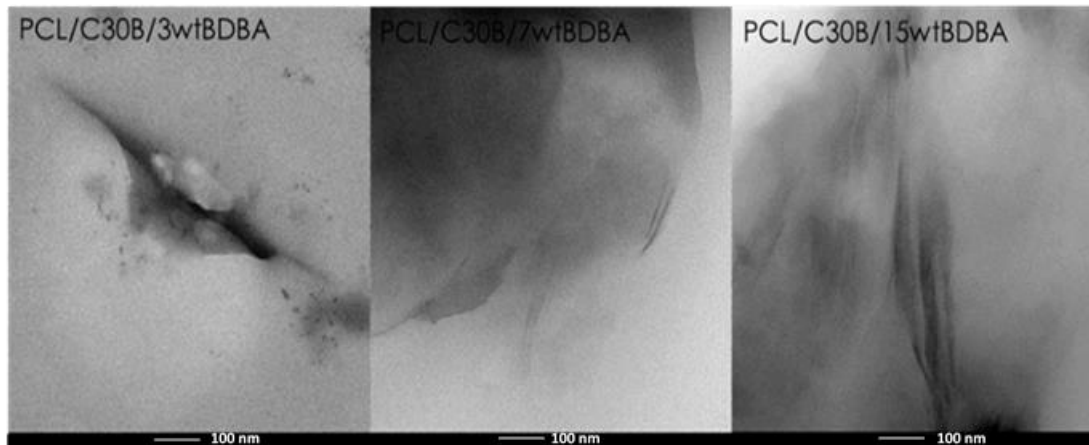
Figure 3. 2. TEM micrographs of PCL-C30B-3wt BDBA, PCL-C30B-7wt BDBA and PCL-C30B-15wt BDBA composites

Light regions indicate the polymer matrix whereas clay platelets can be distinguished by dark zones. Even though separated C30B platelets were detected for PCL-C30B-3wt BDBA, both intercalated and partially exfoliated clay layers exist.

In Figure 3.3, X-ray diffractogram of C15A, PCL and BDBA composites with several ratios of PCL were given.
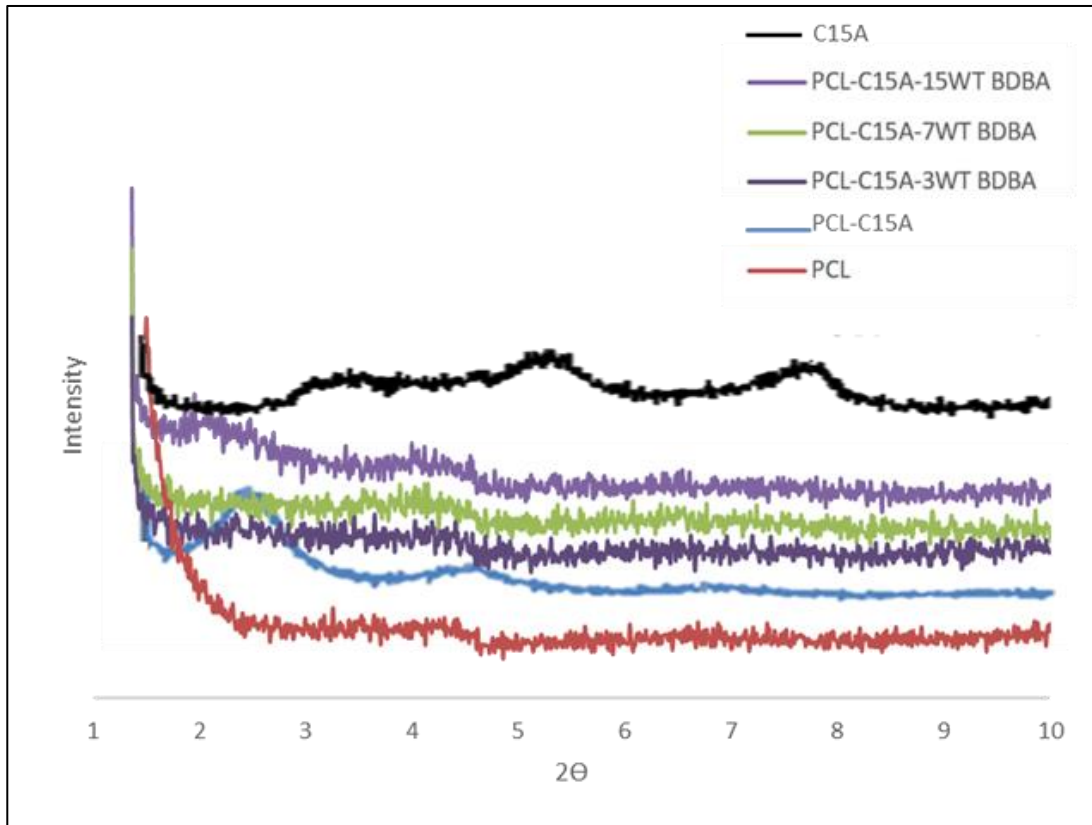
Figure 3. 3. X-ray diffractograms of PCL, C15A, PCL-C15A and PCL-C15A-BDBA composites

The diffractogram of C15A has three distinct peaks at around 2θ=3.34, 5.18 and 7.72° corresponding to an inter-reticular distance of d_{001}=2.64, 1.70 and 1.16 nm, respectively. Except for the PCL-C15A composite, the peaks were almost disappeared for all composites. There is a shift to the lower regions at around 2θ=2.5, 4.5 and 7.0° for PCL-C15A. Probably due to dilation, the peaks of C15A disappeared in the diffractograms of the composites. Dispersion of clay structures into the polymer matrix and the separation of the tactoid structure of C15A can also be considered.

TEM images of PCL-C15A-BDBA composites were represented in Figure 3.4.

26

Figure 3. 4. TEM micrographs of PCL-C15A-3wt BDBA, PCL-C315A-15wt BDBA composites

Tactoid structures of the C15A can be seen from the images especially in the edges of the dark regions. Intercalated and partially exfoliated clay layers exist in the PCL-C15A-BDBA composites.

In Figure 3.5, X-ray diffractogram of BDBA and PCL-BDBA composites with several ratios were given.
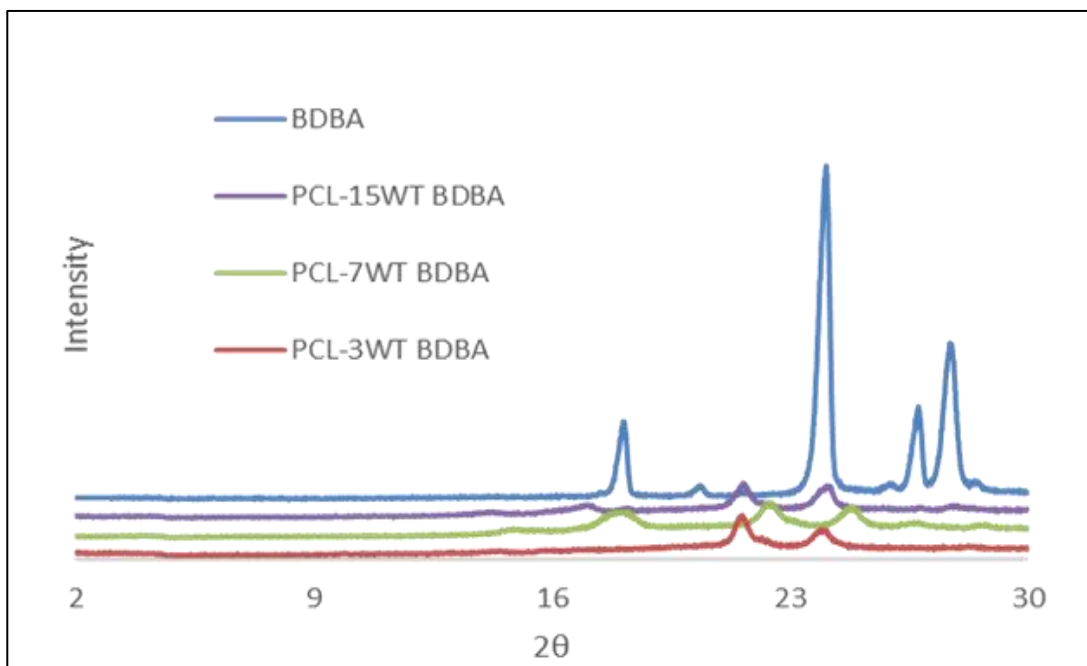
Figure 3. 5. X-ray diffractograms of BDBA and PCL-BDBA composites

The diffractogram of BDBA revealed four distinct peaks at around 2θ=18.21, 24.17, 26.55 and 27.72° related to d_{001}= 0.48, 0.36, 0.33 and 0.32 nm inter-reticular distances, respectively. PCL composites involving different ratios of BDBA showed weak peaks due to dilution of the boron compound in the polymer matrix.

In Figure 3.6, X-ray diffractograms of PCL composites involving C30B and different amounts of BA are given.
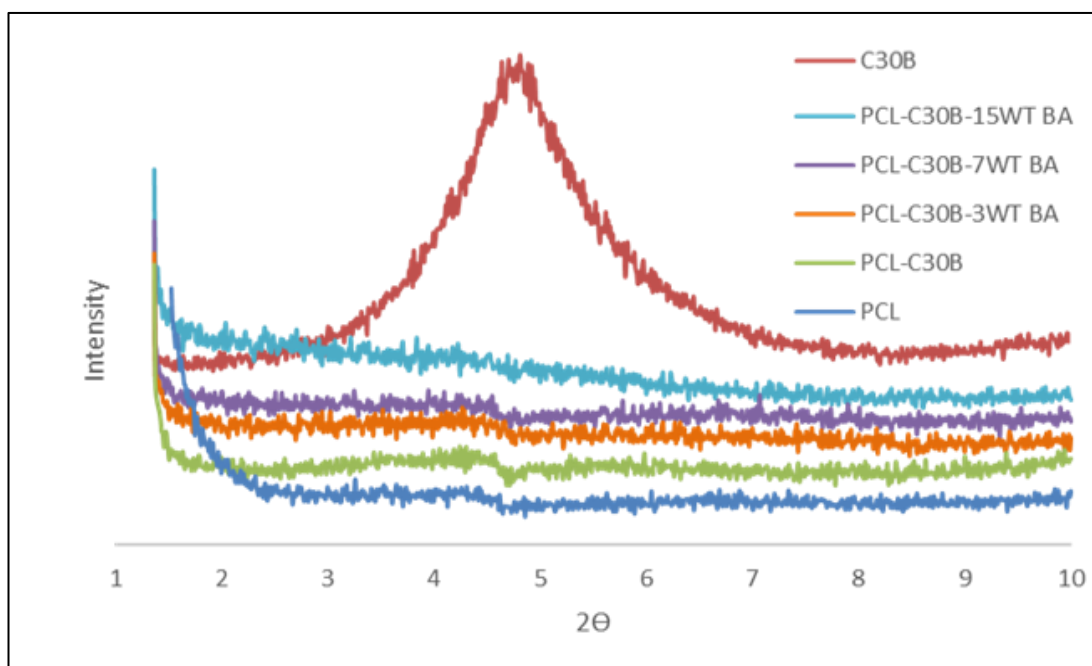
Figure 3. 6. X-ray diffractograms of PCL, C30B, PCL-C30B and PCL-C30B-BA composites

The characteristic peak due to C30B was almost totally disappeared in the diffractograms of all composites of PCL indicating either dispersion of clay in the polymer matrix or well separation of the tactoid structure of clays. TEM images of PCL-C30B-BA composites are represented in Figure 3.7.
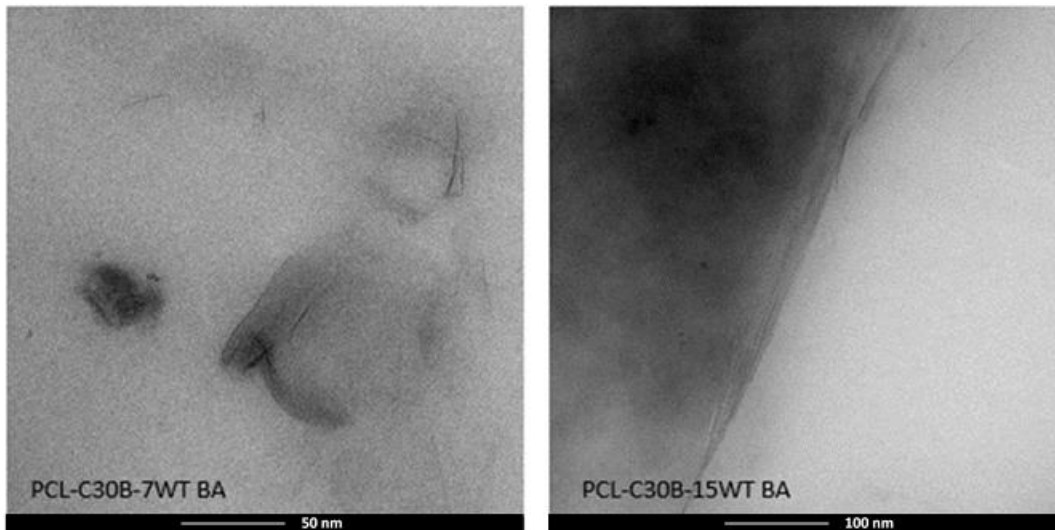
Figure 3. 7. TEM micrographs of PCL-C30B-7wt BA and PCL-C30B-15wt BA composites

Even though separated clay structures were detected, mostly intercalated and partially exfoliated clay layers were generated.

In Figure 3.8, X-ray diffractogram of C15A, BA and PCL composites involving different amount of BA, namely 3, 7 and 15wt% are given.
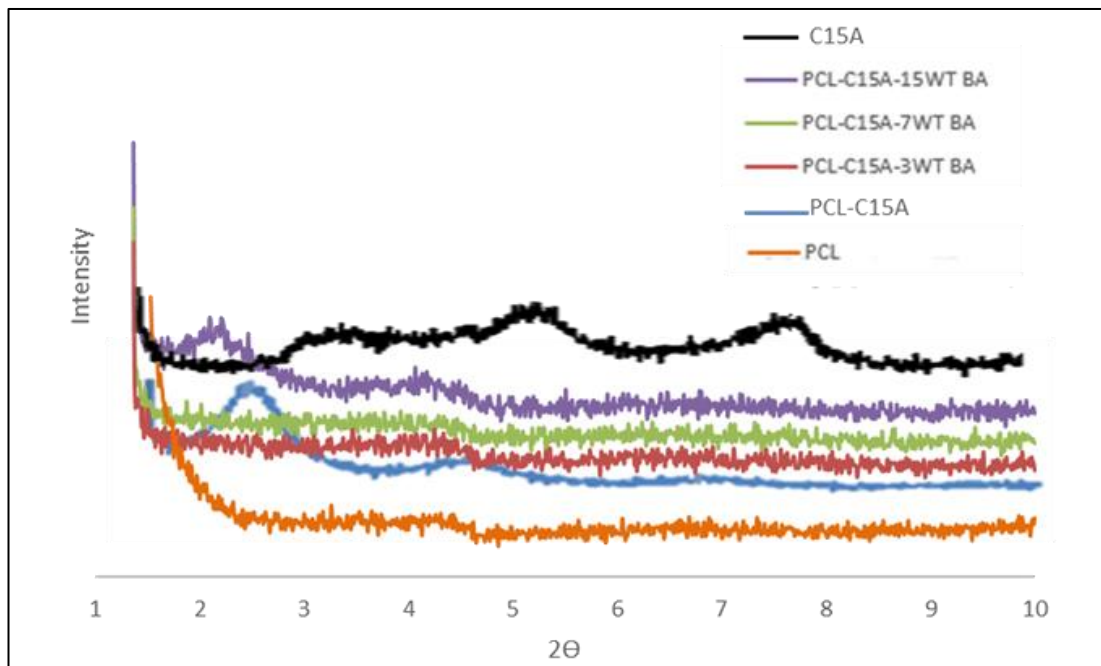
Figure 3. 8. X-ray diffractograms of PCL, C15A, PCL-C15A and PCL-C15A-BA composites

The specific peaks due to C15A were mostly disappeared in diffractograms of PCL, PCL-C15A-3wt BA and PCL-C15A-7wt BA composites indicating dispersion of clay and separation of the layered structure of C15A.

In Figure 3.9, TEM images of PCL-C30B-BA composites are shown.
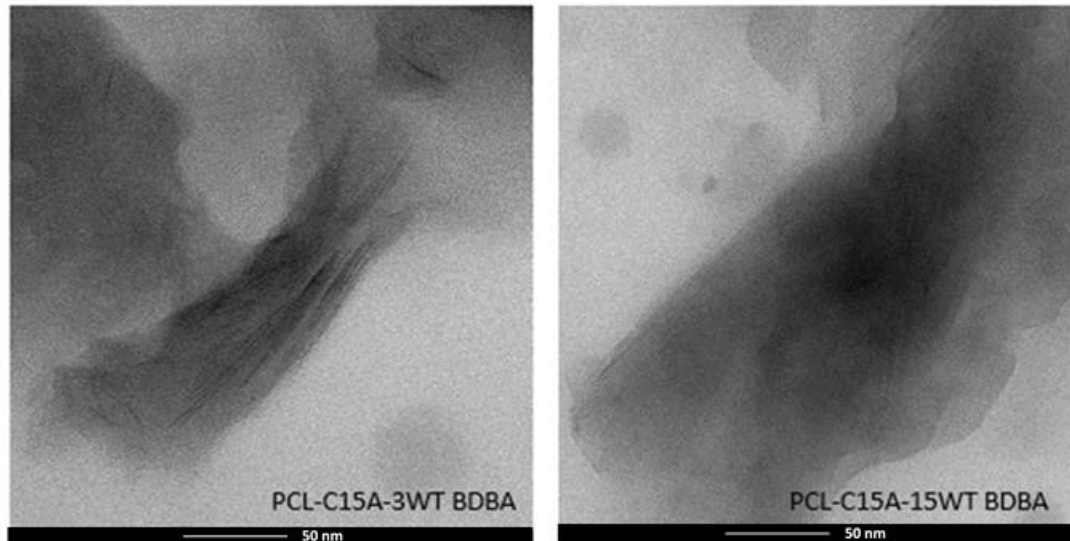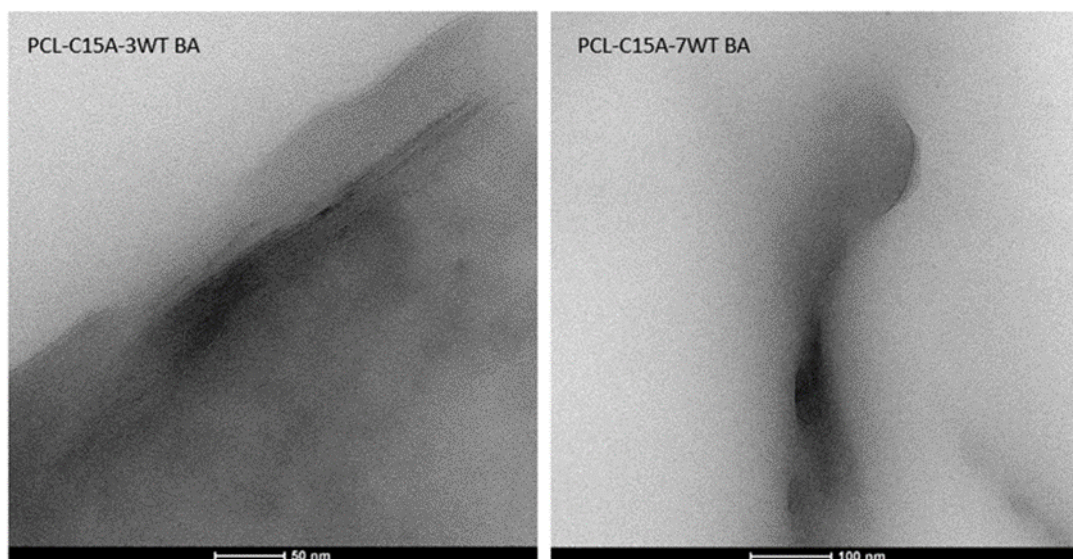
Figure 3. 9. TEM micrographs of PCL-C15A-3wt BA and PCL-C15A-7wt BA composites

Layered structure of C15A can be observed in the images especially in that of the PCL-C15A-3wt BA. TEM micrograms indicated generation of partially intercalated dispersion.

In Figure 3.10, X-ray diffractograms of C30B and PCL composites involving different amounts of ZB are given.
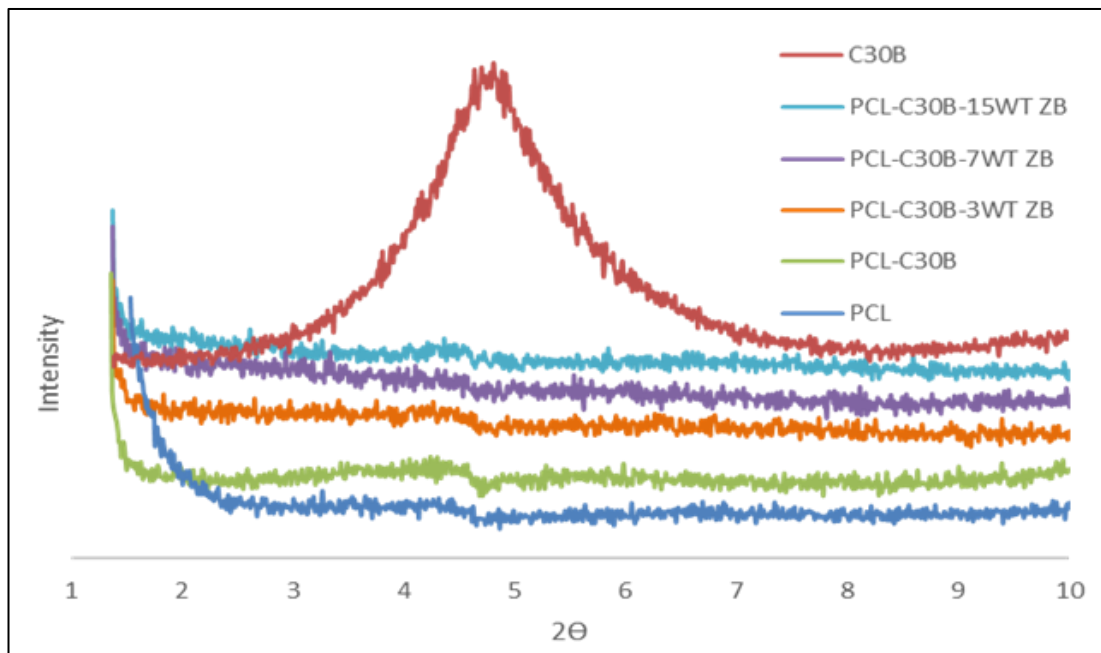
Figure 3. 10. X-ray diffractograms of PCL, C30B, PCL-C30B and PCL-C30B-ZB composites

C30B peak at around $2\Theta=5.0°$ was almost disappeared in the diffractograms of all composites of PCL involving either C30B or ZB. Both dispersion of clay in the polymer matrix and well separation of the tactoid structure of clays can be concluded due to the disappearance of the distinct Bragg peak of C30B. TEM images of PCL-C30B-ZB composites with different boron amounts are presented in Figure 3.11 also supported the XRD findings.
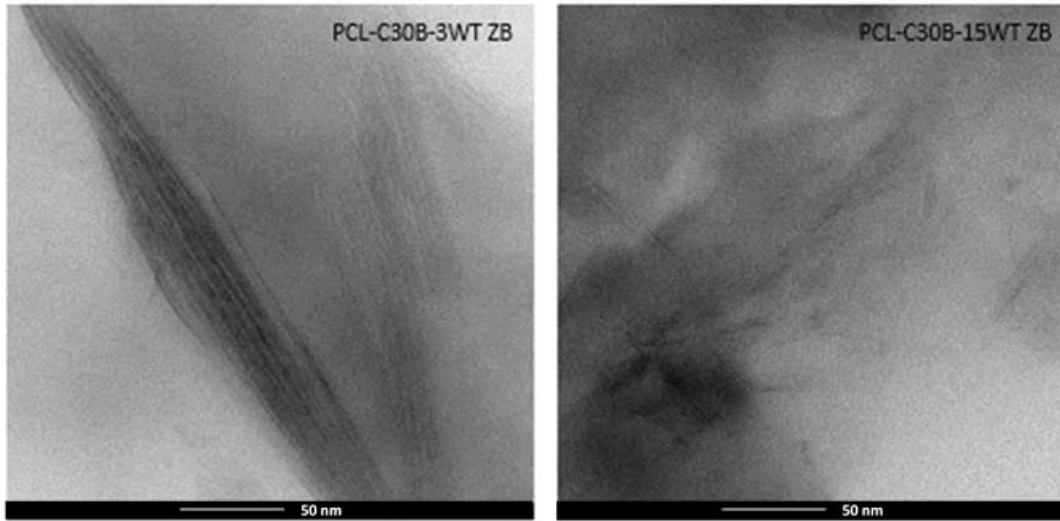
Figure 3. 11. TEM micrographs of PCL-C30B-3wt ZB and PCL-C30B-15wt ZB composites

Tactoid structure of nanoclay was clearly observed in the PCL-C30B-3wt ZB image. On the other hand, in the image of PCL-C30B-15wt ZB, well dispersion of the clays in the PCL matrix was detected.

In Figure 3.12, X-ray diffractograms of C15A and PCL composites involving various amounts of ZB are given.
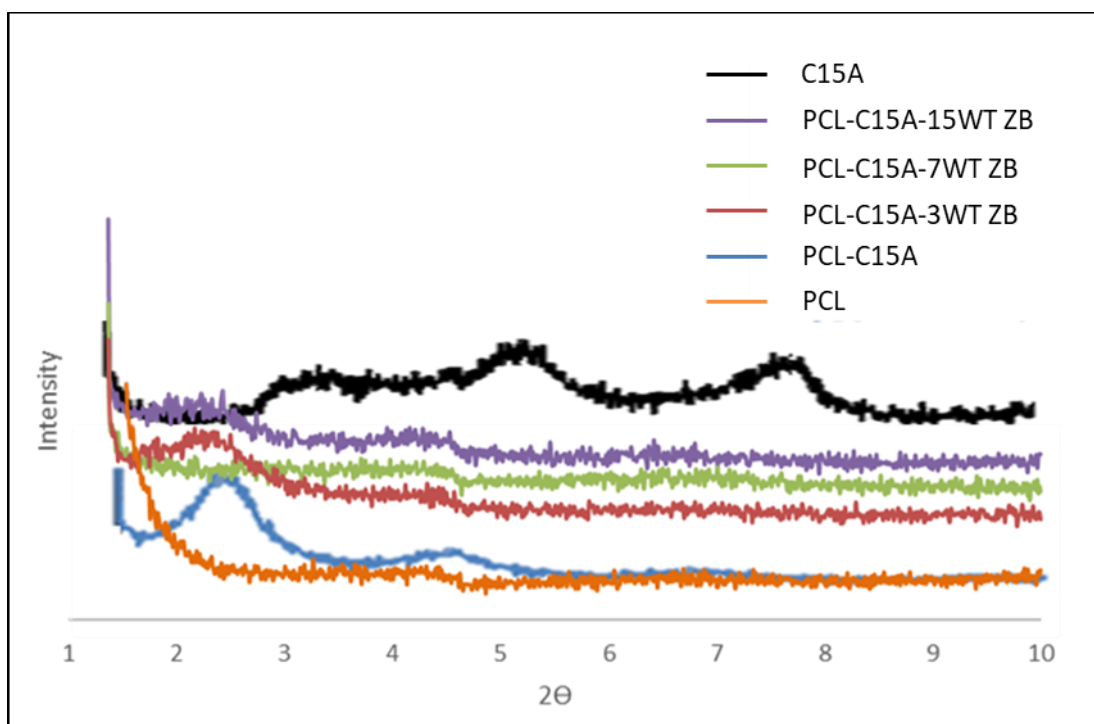
Figure 3. 12. X-ray diffractograms of PCL, C15A, PCL-C15A and PCL-C15A-ZB composites

The specific peaks of C15A were almost disappeared in the diffractograms of PCL and PCL-C15A-ZB composites concluding that dispersion of clay structures and separation of the layered structure of C15A whereas for PLC-C15A, there was a peak at around $2\theta=2.5°$. In Figure 3.13, TEM images of PCL-C15A-ZB composites are presented.
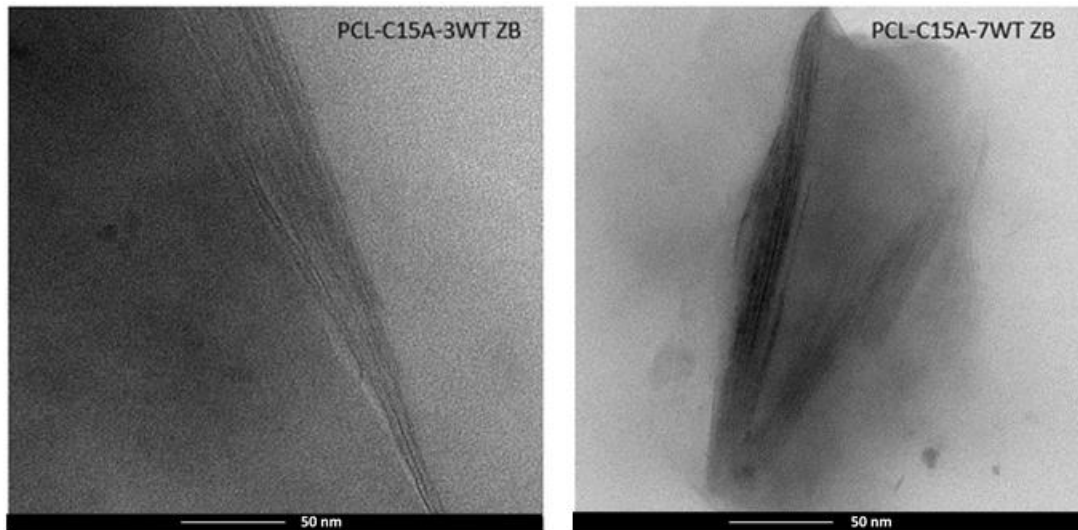
Figure 3. 13. TEM micrographs of PCL-C15A-3wt ZB and PCL-C15A-7wt ZB composite

Layered structure of clays can be distinguished in the images. TEM micrograms indicated generation of partially intercalated dispersion.

3.1.1.1 XRD Patterns of PLA and Its Composites

The diffractograms of C30B and C15A, PLA and its composites involving nanoclay are presented in Figure 3.14.
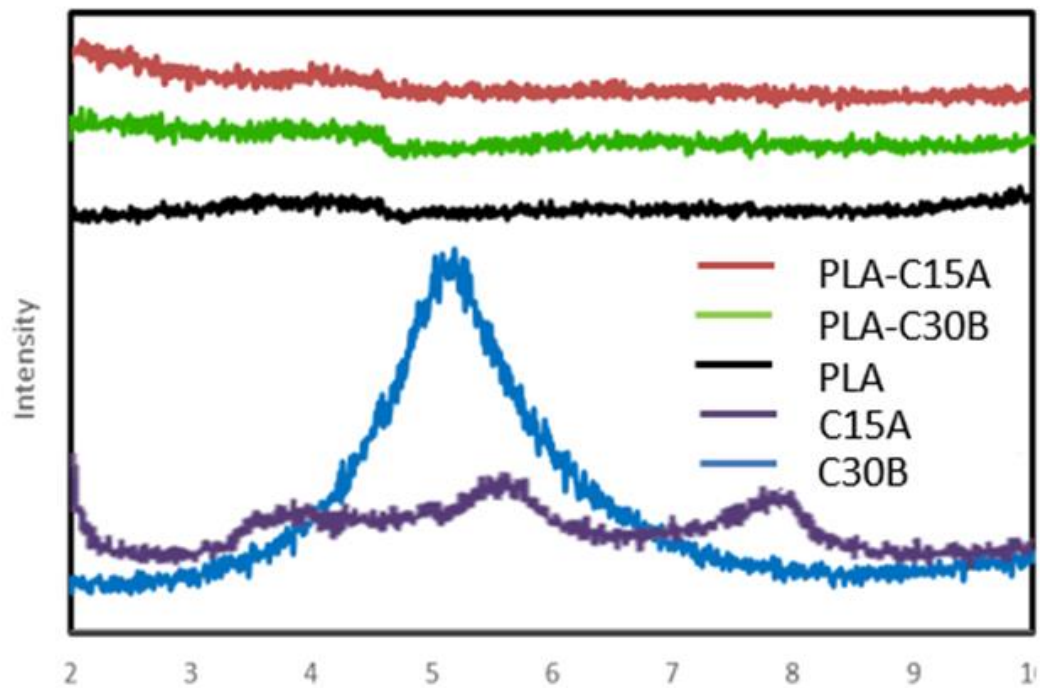
Figure 3. 14. X-ray diffractograms of C30B, C15A, PLA, PLA-C30B and PLA-C15A composites

The specific peaks belonging C30B and C15A were almost totally disappeared for all the composites. The disappearance of the peaks can be associated with both dispersion of clay in the polymer matrices and well separation tactoid structures of clays.

In Figure 3.15, TEM images of PCL-C30B are given.
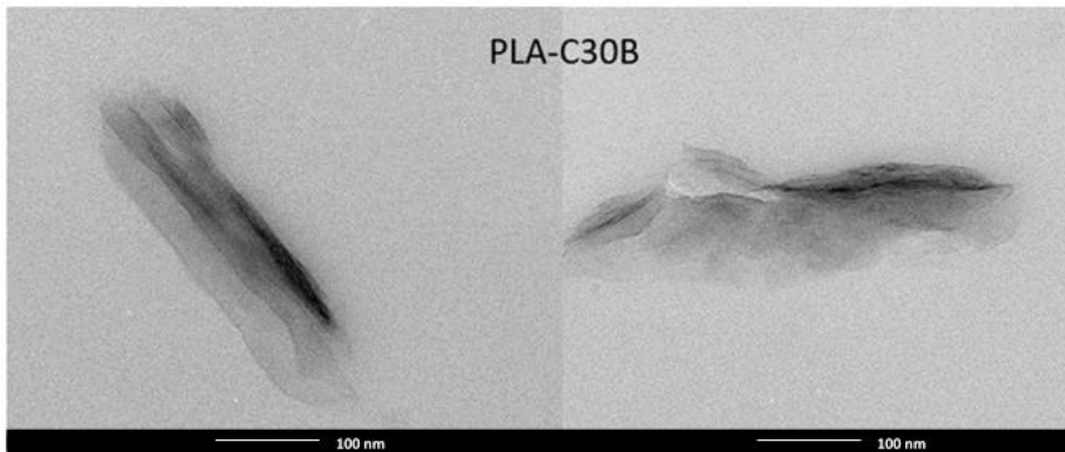
Figure 3. 15. TEM micrographs of PCL-C30B composite

TEM micrograms indicated generation of partially intercalated dispersion.

3.1.1.2 XRD Patterns of PMMA and Its Composites

In Figure 3.16, X-ray diffractograms of C30B and C15A, PMMA and its nanoclay introduced composites are shown.
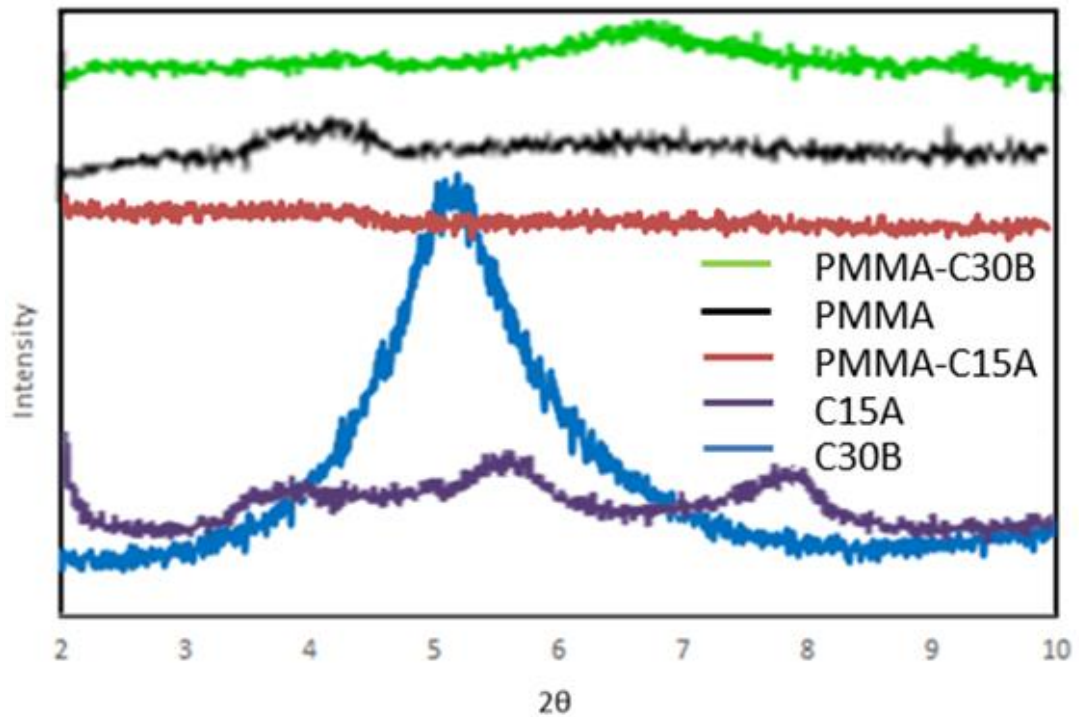
Figure 3. 16. X-ray diffractograms of C30B, C15A, PMMA-C15A, PMMA and PMMA-C30B composites

Characteristics peaks of C30B and C15A were almost totally disappeared for composites of PMMA. Probably due to dilation, dispersion of clay structures in the polymer matrices and the separation of the layered structures of clays were detected.

In Figure 3.17, TEM images of PMMA-C30B and its composites involving BDBA are presented.
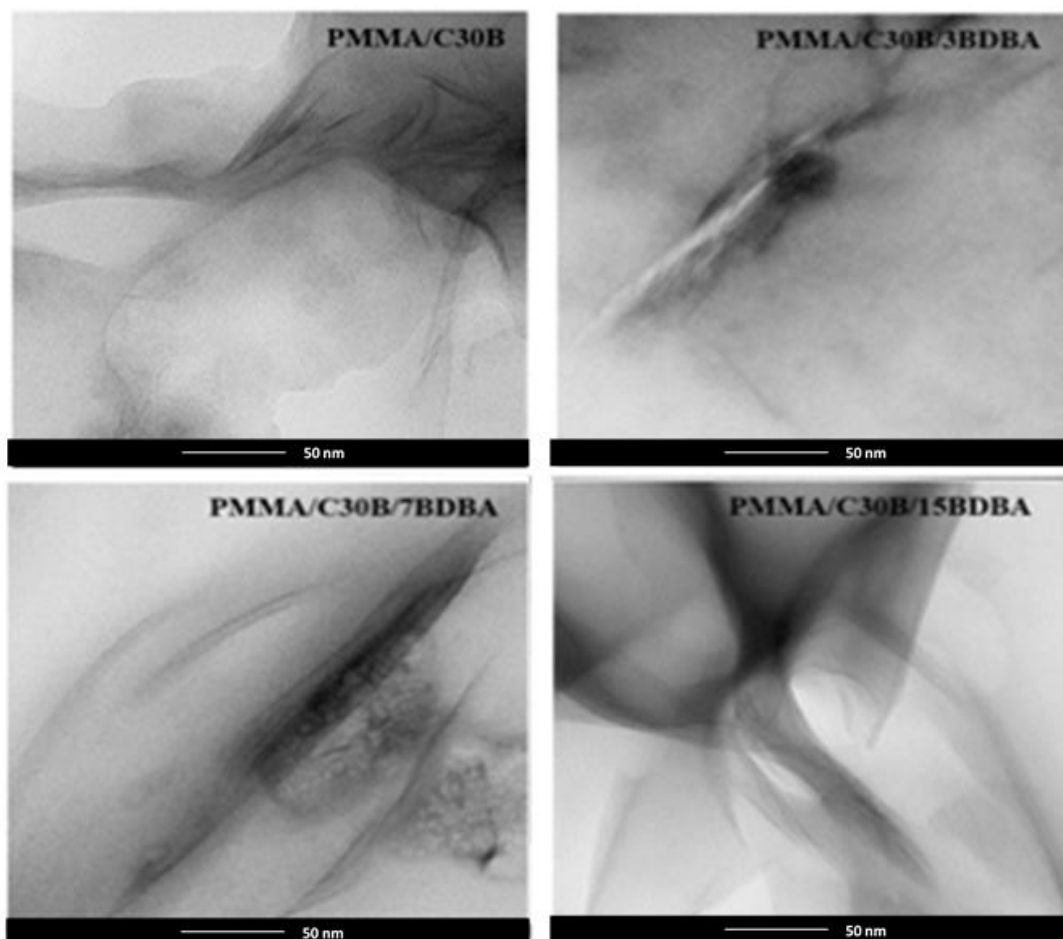
Figure 3. 17. TEM micrographs of PMMA-C30B and PMMA-C30B-BDBA composite

TEM images indicated that dispersion of the C30B was achieved and partially intercalation was generated.

3.1.1.3   XRD Patterns of PNBMA and Its Composites

X-ray diffractogram of C30B and C15A, PnBMA and its composites involving nanoclay are shown in Figure 3.18.
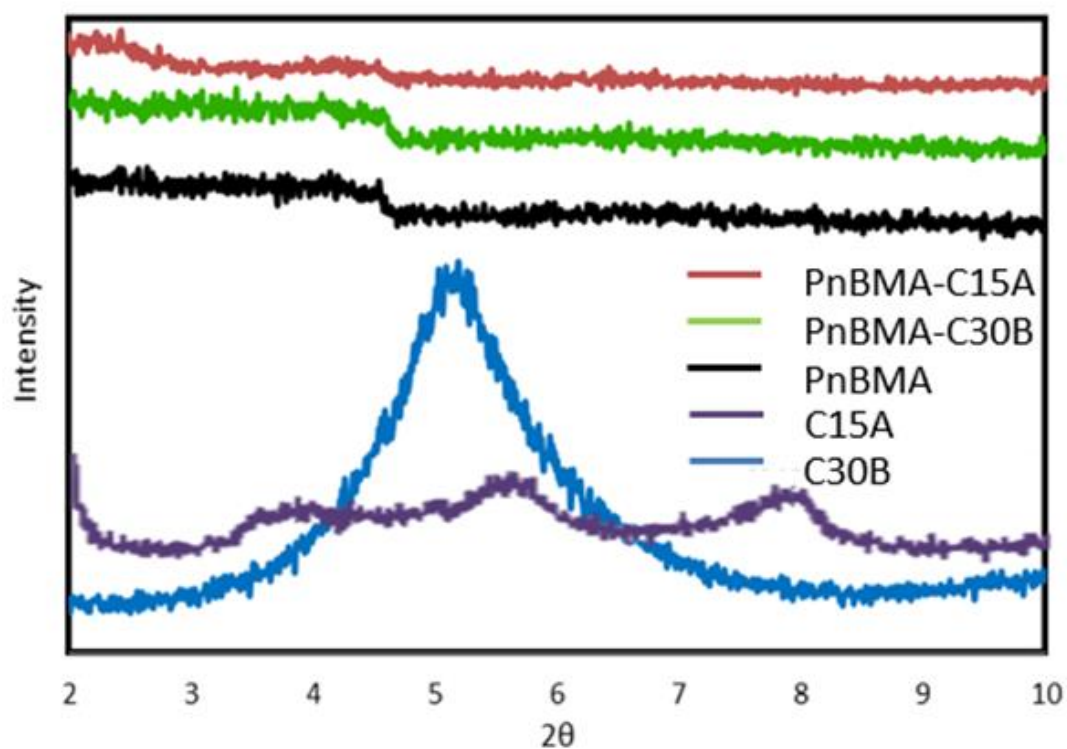
Figure 3. 18. X-ray diffractograms of C30B, C15A, PnBMA, PnBMA-C30B and PnBMA-C15A composites

Distinct peaks of C30B and C15A peaks were almost totally disappeared in the diffractograms of PnBMA composites. Probably due to dilation, dispersion of clay in the polymer matrix and the separation of the layered structures of clays were interpreted.

TEM analyses were also performed to support the XRD results. In Figure 3.19, TEM images of PnBMA-C30B-BDBA composites are given.
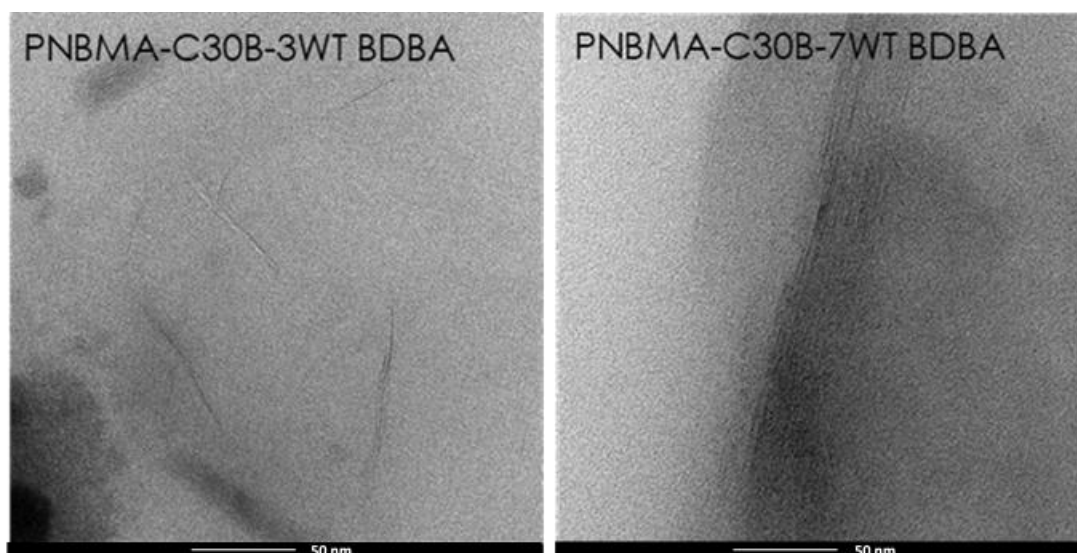
Figure 3. 19. TEM micrographs of PnBMA-C30B-3wt BDBA and PnBMA-C30B-7wt BDBA composites

Layered structure of clays can be observed. TEM micrograms indicated that partially intercalated dispersion was generated for the PnBMA composites.

3.1.2   SEM Results of Electrospun Fibers

Electrospun fibers of PCL were obtained changing the experimental parameters such as polymer concentration, solvent systems and BDBA content. DCM/DMF was used as solvent system. Bead-free PCL fibers could not be obtained. The morphology of the fibers was examined by SEM analyses.

3.1.2.1   SEM Micrograms of PCL and Its Composite Fibers

The morphology of the electrospun fibers were analyzed by SEM. In Figure 3.20, SEM images of 5, 10 and 20 wt% PCL nanofibers in DCM/DMF solvent systems volume ratio 80:20 (v/v) at low and high magnifications are given.
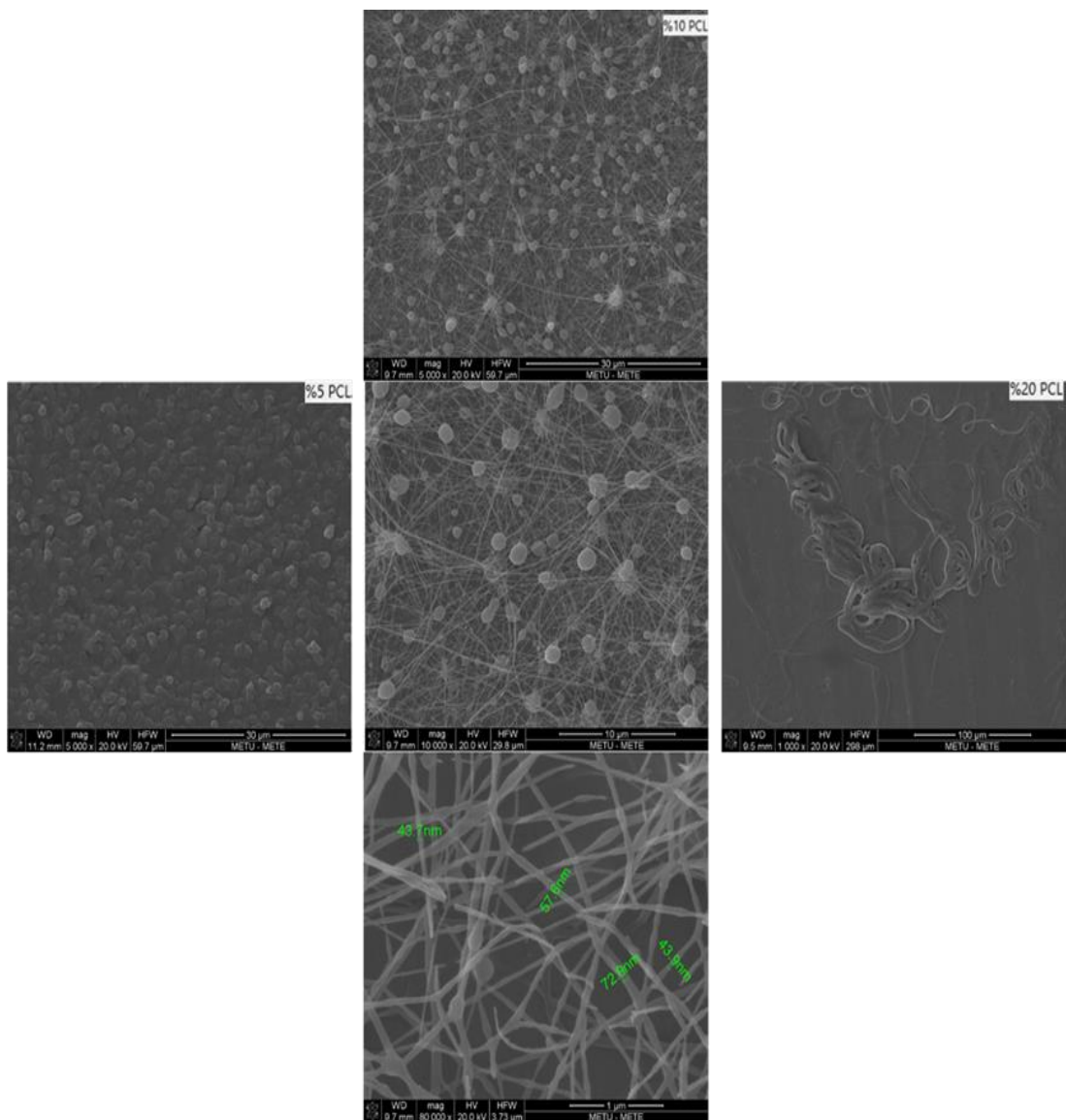
Figure 3. 20. SEM images of 5, 10 and 20 wt% PCL composites and nanofibers in DCM/DMF solvent systems volume ratio 80:20 (v/v)

As it can be seen in Figure 3.20, for the low (%5wt) and high (%20wt) polymer concentrations, the fiber structure was not achieved. In the low amount, accumulated structure was detected whereas thread as texture was obtained at high concentration.

Additionally, for %10wt PCL, even though there was intense beads and bad quality, the fiber structure was succeeded.

SEM images of 15wt% PCL nanofibers in various volume ratios of DCM/DMF solvent systems are given In Figure 3.21.
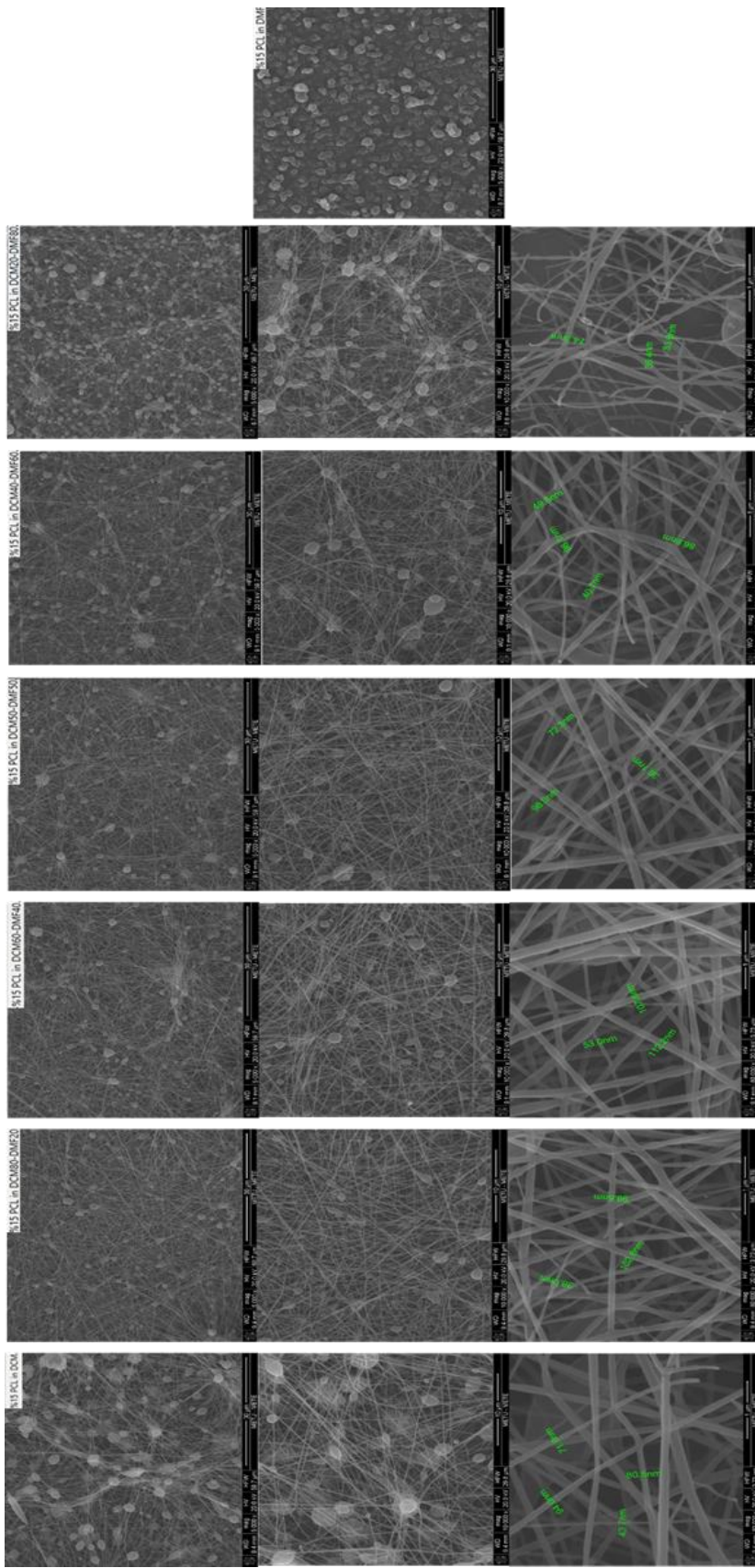
Figure 3. 21. SEM images of 15 wt% PCL nanofibers in DCM/DMF solvent systems volume ratio 0:100, 80:20, 60:40, 50:50, 40:60, 20:80 and 100:0 (v/v), respectively

As the volume ratio of DMF was increased keeping the concentration of PCL constant (15 wt%), the bead intense was also raised. Especially for 40:60 and 20:80 (v/v) DCM/DMF, the fiber quality was disrupted. When the solvent was just DMF, fiber structure was totally disappeared. It can be concluded that, the least number of beads was obtained for the 80:20 (v/v) DCM/DMF solvent system.

SEM images of 15 wt% PCL-C30B-BDBA nanofibers involving different amounts of boron compound are given in Figure 3.22.
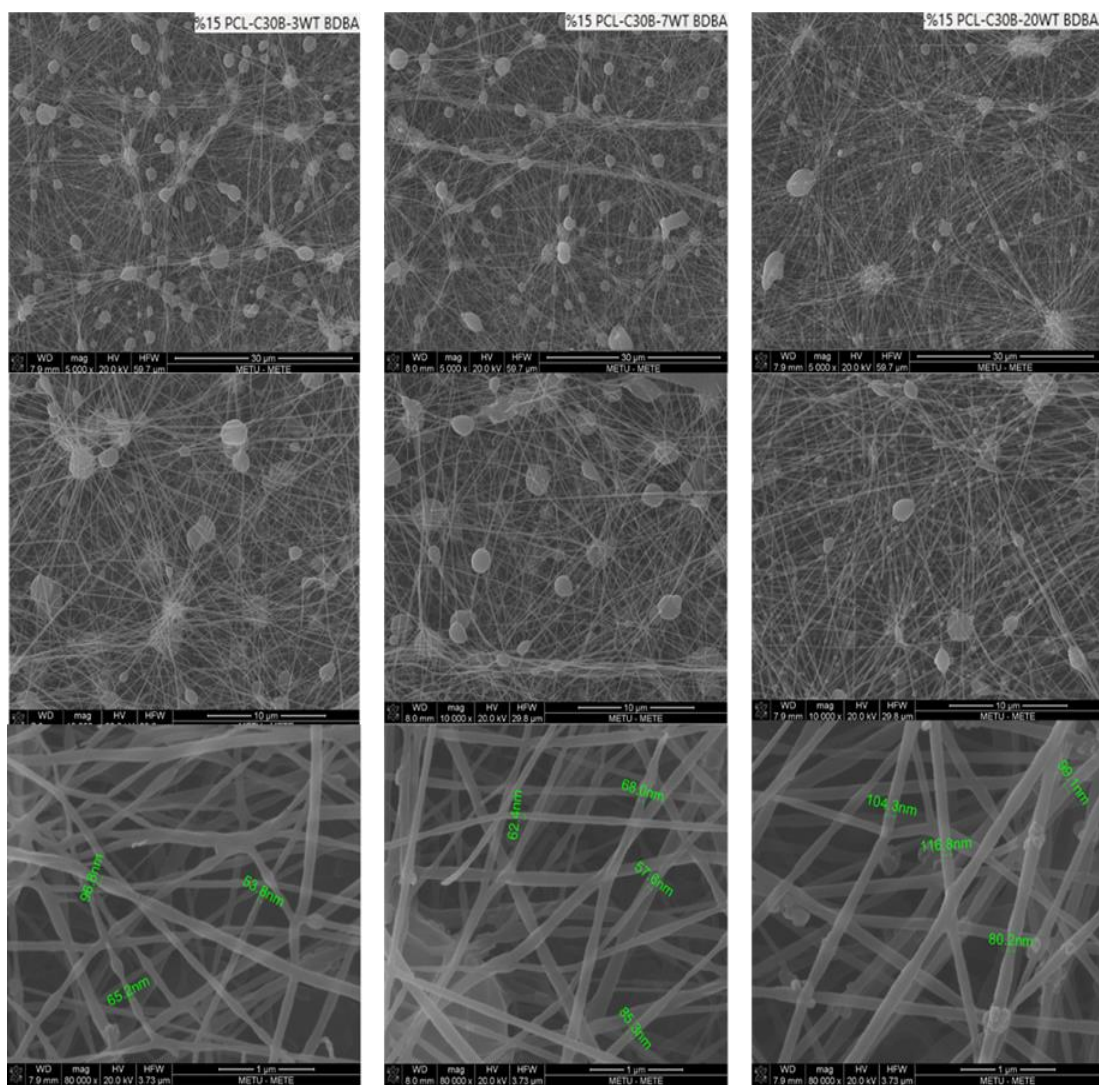
Figure 3. 22. SEM images of 15 wt% PCL-C30B-3WT BDBA, PCL-C30B-7WT BDBA and PCL-C30B-15WT BDBA nanofibers in DCM/DMF solvent system with volume ratio 80:20 (v/v), respectively

As the amount of BDBA was increased, thinner fibers were obtained. Moreover, bead intense was relatively low for the highest amount of BDBA, again.

3.2 Thermal Results

Thermal characteristics of PCL and PLA and their clay and boron involving composites were studied by thermogravimetry and direct pyrolysis mass spectrometry techniques.

3.2.1 TGA Results

3.2.1.1 TGA Curves of PCL and Its Composites

TGA and DTG curves of neat PCL, PCL-C30B and BDBA involving composites are given in Figure 3.23.
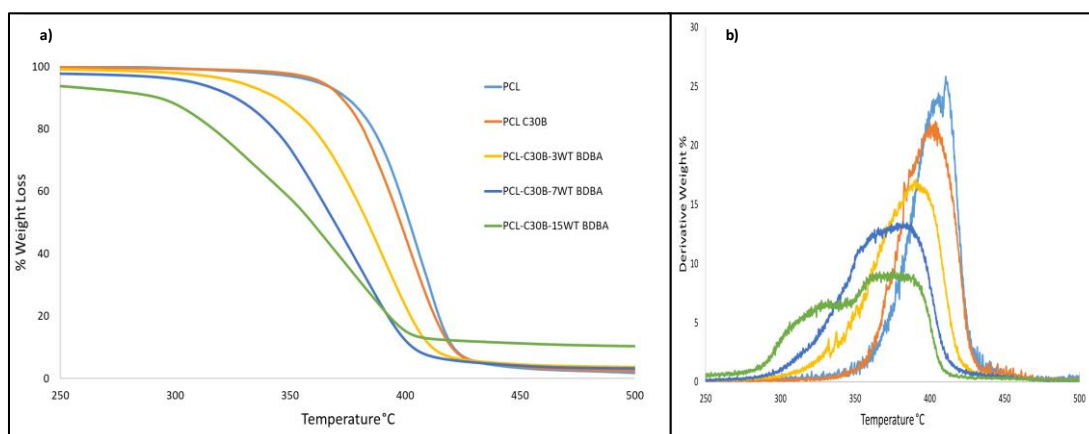
Figure 3. 23. a) TGA and b) DTG curves of neat PCL, PCL-C30B, PCL-C30B composites with 3, 7 and 15wt% BDBA

PCL started to decompose at around 361.6 °C. Its thermal degradation was shifted to lower temperatures in the presence of C30B. The shift to lower temperatures of became more pronounced with the addition of BDBA. Increase in amount of BDBA added did not have any further effect.

The temperatures at which 5% ($T_{5\%}$), 10% ($T_{10\%}$), maximum weight losses (T_{max}) took place and char yield ratio are summarized in Table 3.1.

Table 3. 1 TGA data of neat PCL, PCL-C30B, PCL-C30B composites with 3, 7 and 15wt% BDBA

	$T_{5\%}$	$T_{10\%}$	T_{max}	% char yield
PCL	361.3	374.3	404.4	1.4
PCL-C30B	363.5	372.2	403.7	1.7
PCL-C30B-3wt BDBA	327.3	344.0	390.8	3.5
PCL-C30B-7wt BDBA	304.9	325.1	382.0	2.6
PCL-C30B-15wt BDBA	310.5	331.3	375.9	7.1

TGA and DTG curves of neat PCL, PCL-C15A and BDBA involving composites are given in Figure 3.24.

Figure 3. 24. a) TGA and b) DTG curves of neat PCL, PCL-C15A, PCL-C15A composites with 3, 7 and 15wt% BDBA

Thermal decomposition of PCL again shifted to lower temperatures in the presence of C15A. The shift to lower temperatures became more significant upon addition of BDBA.

The temperatures at which 5% ($T_{5\%}$), 10% ($T_{10\%}$), maximum weight losses (T_{max}) took place and char yield ratio are summarized in Table 3.2.

Table 3. 2 TGA data of neat PCL, PCL-C15A, PCL-C15A composites with 3, 7 and 15wt% BDBA

	$T_{5\%}$	$T_{10\%}$	T_{max}	% char yield
PCL	361.3	374.3	404.4	1.4
PCL-C15A	351.8	362.8	394.5	2.5
PCL-C15A-3wt BDBA	325.5	340.0	384.9	3.7
PCL-C15A-7wt BDBA	302.2	325.8	381.6	2.0
PCL-C15A-15wt BDBA	320.0	335.0	376.9	5.2

TGA and DTG curves of neat PCL, PCL-C30B and BA involving composites are shown in Figure 3.25.
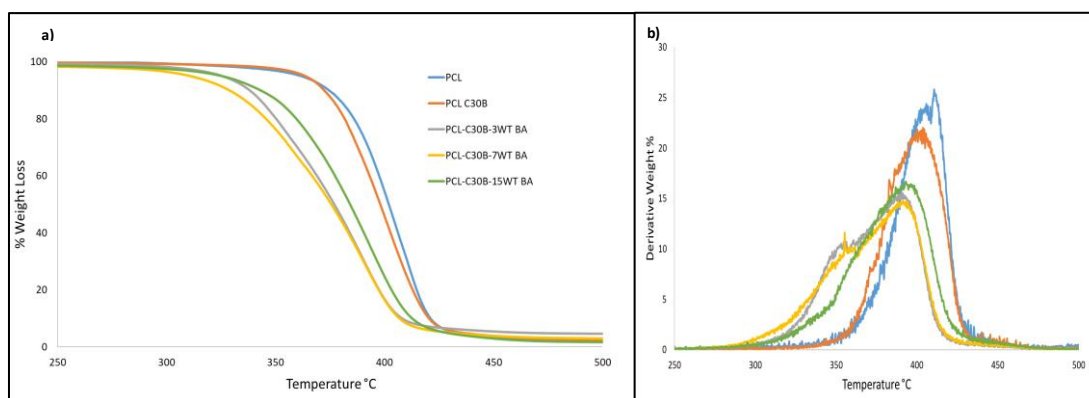
Figure 3. 25. a) TGA and b) DTG curves of neat PCL, PCL-C30B, PCL-C30B composites with 3, 7 and 15wt% BA

When BA was added into PCL-C30B matrix, thermal stability of the composites was significantly decreased.

The temperatures at which 5% ($T_{5\%}$), 10% ($T_{10\%}$), maximum weight losses (T_{max}) took place and char yield ratio are summarized in Table 3.3.

Table 3. 3 TGA data of neat PCL, PCL-C30B, PCL-C30B composites with 3, 7 and 15wt% BA

	$T_{5\%}$	$T_{10\%}$	T_{max}	% char yield
PCL	361.3	374.3	404.4	1.4
PCL-C30B	363.5	372.2	403.7	1.7
PCL-C30B-3wt BA	325.6	338.0	390.3	4.5
PCL-C30B-7wt BA	310.9	328.8	391.1	2.8
PCL-C30B-15wt BA	325.5	343.1	393.2	1.5

In Figure 3.26, TGA and DTG curves of PCL composites involving C15A and BA are presented.
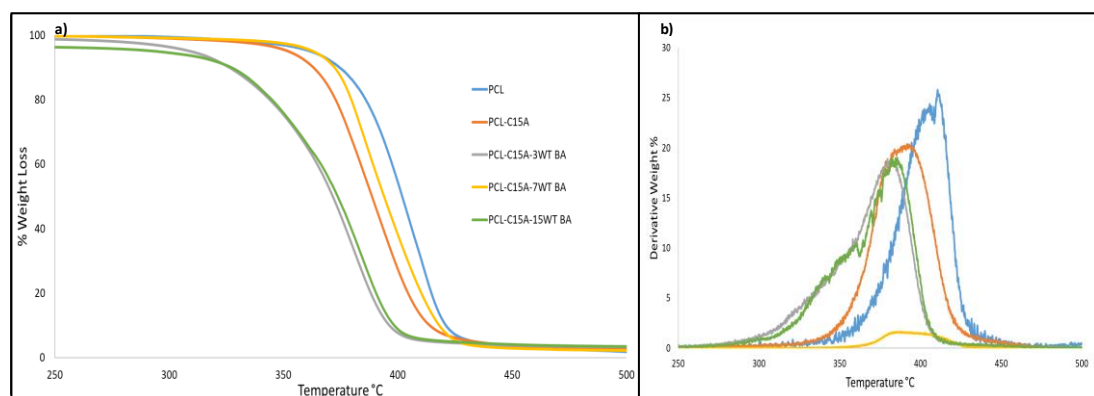
Figure 3. 26. a) TGA and b) DTG curves of neat PCL, PCL-C15A, PCL-C15A composites with 3, 7 and 15wt% BA

Similar results were obtained when C15A and BA with various amounts were added to PCL. Yet the decrease in thermal stability of PCL was more pronouncedly compared to PCL-C15A and PCL-C15A-7wt BA.

The temperatures at which 5% ($T_{5\%}$), 10% ($T_{10\%}$), maximum weight losses (T_{max}) took place and char yield ratio are presented in Table 3.4.

Table 3. 4 TGA data of neat PCL, PCL-C15A, PCL-C15A composites with 3, 7 and 15wt% BA

	$T_{5\%}$	$T_{10\%}$	T_{max}	% char yield
PCL	361.3	374.3	404.4	1.4
PCL-C15A	351.8	362.8	394.5	2.5
PCL-C15A-3wt BA	309.4	326.4	382.5	3.2
PCL-C15A-7wt BA	362.7	372.1	385.3	1.8
PCL-C15A-15wt BA	293.8	326.9	385.7	3.2

TGA and DTG curves of neat PCL, PCL-C30B and ZB involving composites are shown in Figure 3.27.
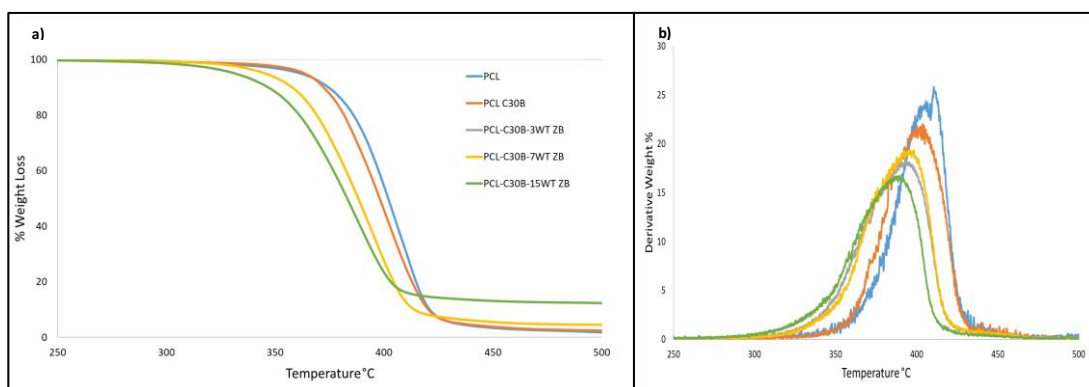
Figure 3. 27. a) TGA and b) DTG curves of neat PCL, PCL-C30B, PCL-C30B composites with 3, 7 and 15wt% ZB

Thermal stability of PCL shifted to lower temperatures upon addition of C30B and ZB.

The temperatures at which 5% ($T_{5\%}$), 10% ($T_{10\%}$), maximum weight losses (T_{max}) took place and char yield ratio are summarized in Table 3.5.

Table 3. 5 TGA data of neat PCL, PCL-C30B, PCL-C30B composites with 3, 7 and 15wt% ZB

	$T_{5\%}$	$T_{10\%}$	T_{max}	% char yield
PCL	361.3	374.3	404.4	1.4
PCL-C30B	363.5	372.2	403.7	1.7
PCL-C30B-3wt ZB	342.9	354.8	390.5	4.6
PCL-C30B-7wt ZB	345.3	357.8	398.3	4.3
PCL-C30B-15wt ZB	331.5	346.8	389.1	12.2

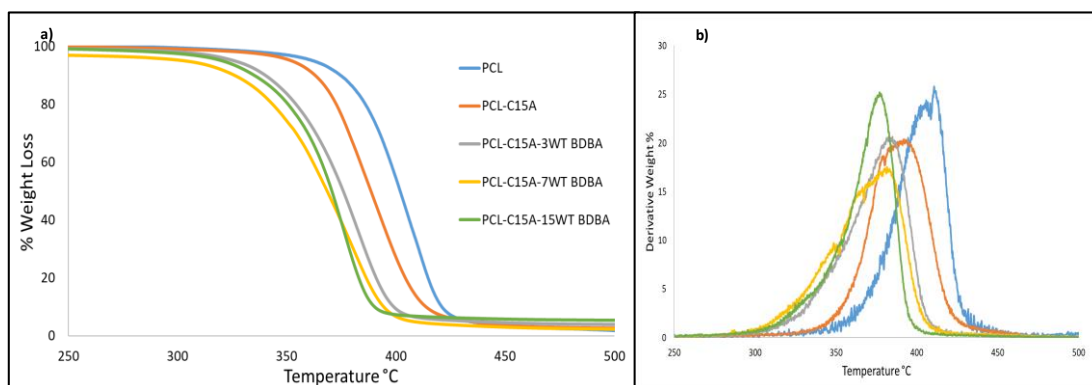In Figure 3.28, TGA and DTG curves of PCL composites involving C15A and ZB are given.
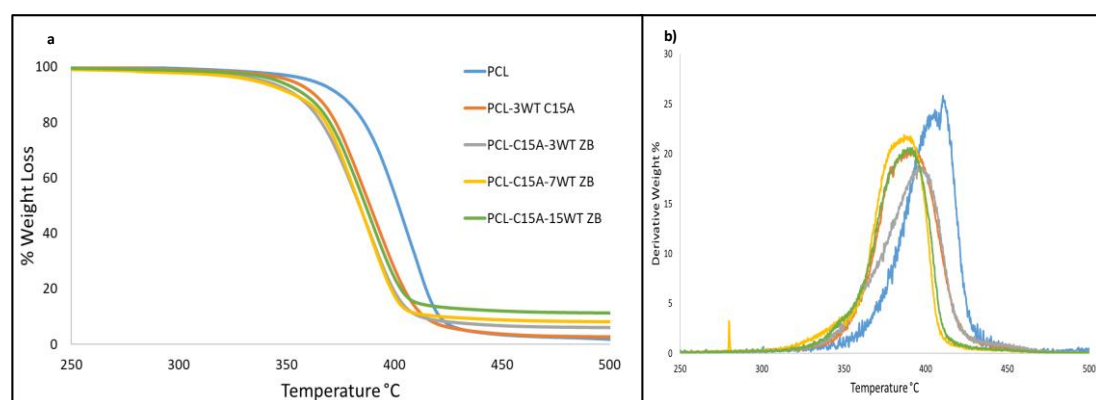
Figure 3. 28. a) TGA and b) DTG curves of neat PCL, PCL-C15A, PCL-C15A composites with 3, 7 and 15wt% ZB

Decrease in thermal stability of PCL was detected in ZB involving composites. Thermal stability was not directly proportional with ZB amount.

The temperatures at which 5% ($T_{5\%}$), 10% ($T_{10\%}$), maximum weight losses (T_{max}) took place and char yield ratio are summarized in Table 3. 6.

Table 3. 6 TGA data of neat PCL, PCL-C15A, PCL-C15A composites with 3, 7 and 15wt% ZB

	$T_{5\%}$	$T_{10\%}$	T_{max}	% char yield
PCL	361.3	374.3	404.4	1.4
PCL-C15A	351.8	362.8	394.5	2.5
PCL-C15A-3wt ZB	339.1	354.0	396.9	5.8
PCL-C15A-7wt ZB	334.9	353.0	389.9	7.9
PCL-C15A-15wt ZB	345.5	358.3	390.6	11.0

3.2.2 DP-MS Results

The effects of clays and boron compounds on thermal degradation of polyesters and its composites were also studied by Direct Pyrolysis Mass Spectrometry. Pyrolysis mass spectrum of neat polyesters, boron compounds; BDBA, BA, ZB and also clays: C30B and C15A, polyester/boron and polyester/clay/boron composites involving various amounts of boron content were recorded as a function of temperature and analyzed systematically. Total Ion Current (TIC) curves and the pyrolysis mass spectra recorded at the maxima of the TIC curves were studied systematically.

3.2.2.1 Clays

The total ion current curve and mass spectra recorded at peak maxima present in the TIC curves of C30B are given in Figure 3.29.
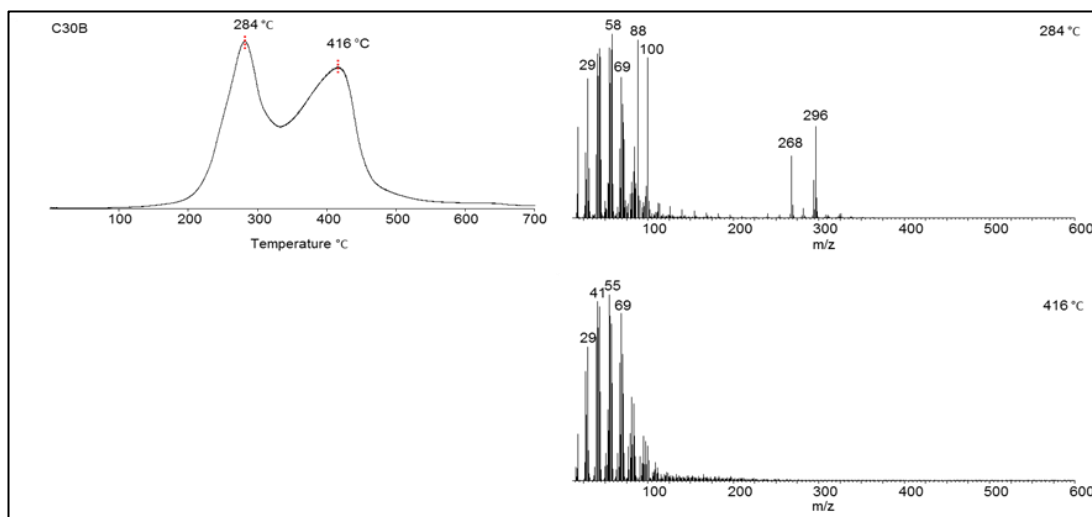
Figure 3. 29. Total ion current curve and mass spectrum of C30B at the peak maxima

The TIC curve of C30B shows two peaks, at around 284 and 416°C. The mas spectra recorded at around 284 °C show the base peak at 58 Da may be due to $C_2H_4NH(CH_3)$ and show diagnostic peaks for amines such as those at 88 and 100 Da. The peak at 296 Da that can directly be attributed to $C_{18}H_{37}(CH_3)NHCH_2$, and/or $C_{16}H_{31}N(CH_2)C_2H_4OH$ fragments. For C30B, the mass spectra recorded at elevated temperatures, at around 416°C showed slightly different fragmentation pattern than those recorded around 284°C. The peaks may be related to degradation of high molar mass hydrocarbons.

In Figure 3.30 the total ion current curve and its mass spectra recorded at peak maxima of C15A are presented.
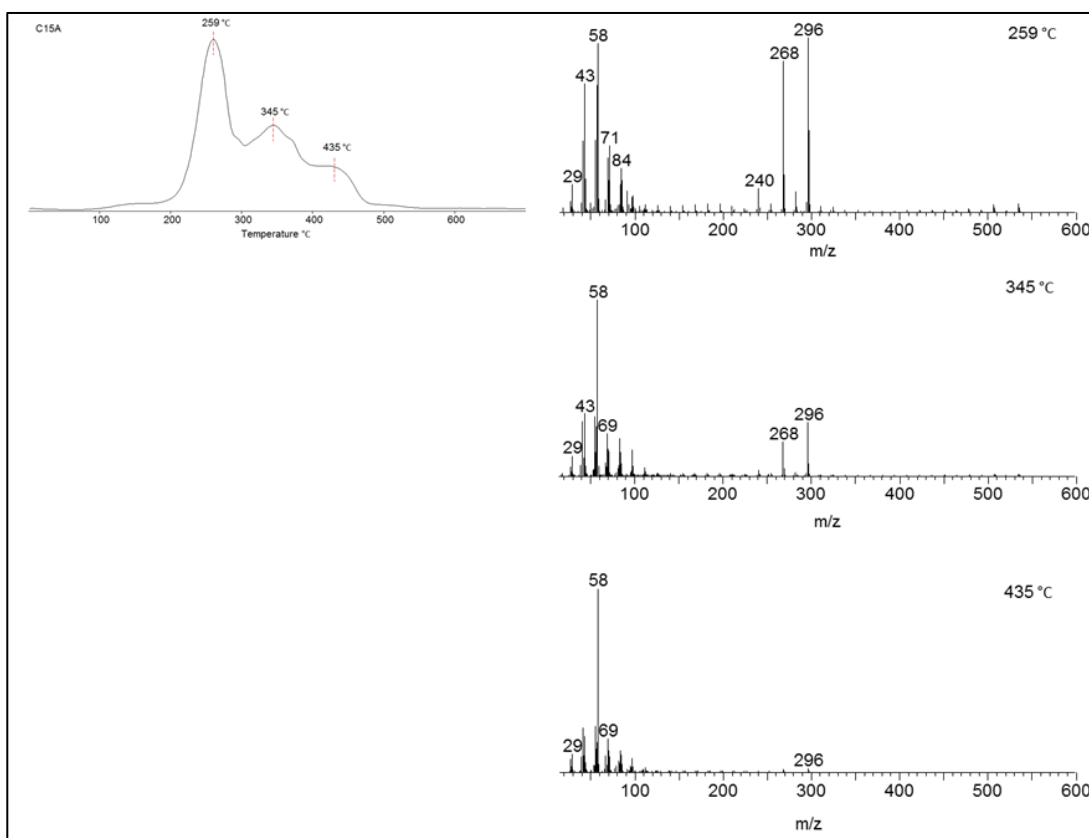
Figure 3. 30. Total ion current curve and mass spectra of C15A at the peak maxima

The TIC curve of C15A shows three peaks, at around 259, 345 and 435°C. The mass spectra recorded at around 259 °C shows the base peak is at 296 Da that can directly be attributed to $C_{18}H_{37}N(CH_3)_2$ fragment. Two weaker peaks at around 345 and 435°C, are also present in the total ion current, TIC, curve of C15A.

56

3.2.2.2   PCL and Its Composites

The TIC, curves of PCL, PCL-C15A and PCL-C30B composites are given in Figure 3.31. The pyrolysis mass spectra recorded at the maximum of the peaks present in the TIC curves are also included in the figure.
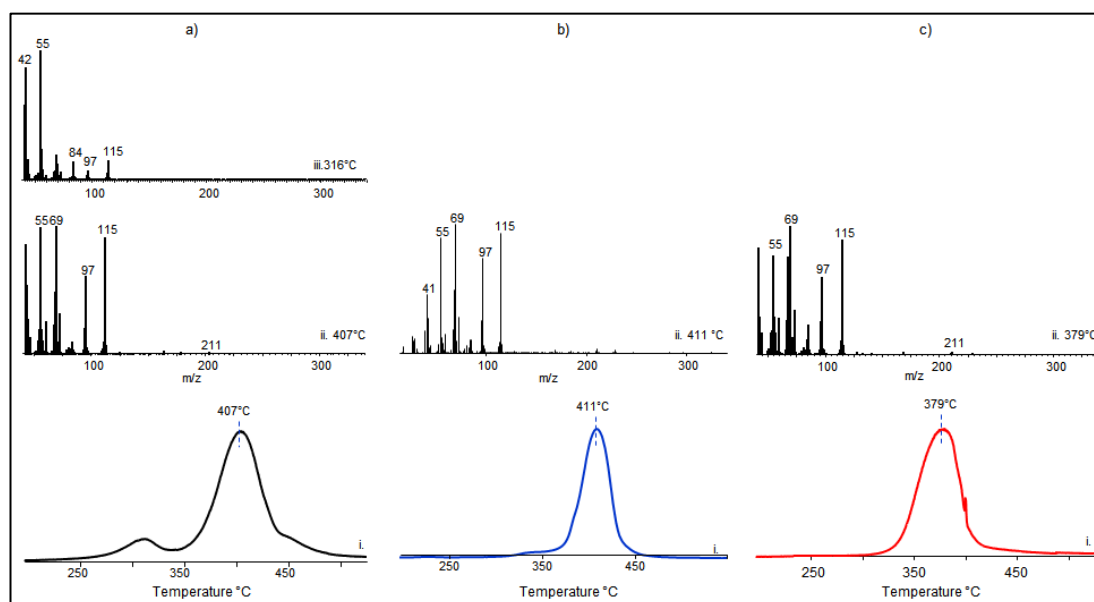
Figure 3. 31. i. TIC curves and ii and ii. pyrolysis mass spectra recorded during the pyrolysis of a) PCL, b) PCL-C15A and c) PCL-C30B

TIC curve of PCL shows two peaks at around 316 and 407 °C. The pyrolysis mass spectra recorded at low temperature peak maximum indicated that generation of products due to thermal degradation of low molar mass oligomers. On the other hand the high temperature peak at around 407 °C was attributed to generation of products by random chain scission processes followed by depropagation step yielding mainly the monomer, and low mass fragments. In the presence of nanoclays, the low temperature peak in the TIC curve of PCL was disappeared most probably due to the solution mixing process. Although, thermal decomposition of PCL-C15A occurred

at slightly higher temperatures, a remarkable decrease in thermal stability of PCL-C30B was detected. Yet, the pyrolysis mass spectra of PCL and its composites were quite similar. Only small variations in the relative intensities of low mass fragments were detected. In Figure 3.32 single ion evolution profiles of characteristic and/or abundant products, namely, C_4H_7 (55 Da), C_5H_9 (69 Da), C_5H_9CO (97 Da) and $C_5H_{10}CO_2H$ (115 Da) are depicted. In addition, single ion pyrograms of the most abundant pyrolysis product of organic modifiers, $C_{18}H_{37}N(CH_3)CH_2$ (296 Da) for C15A and $C_{18}H_{37}NHCH_2CH_2$ (296 Da) for C30B are also included in the figure.
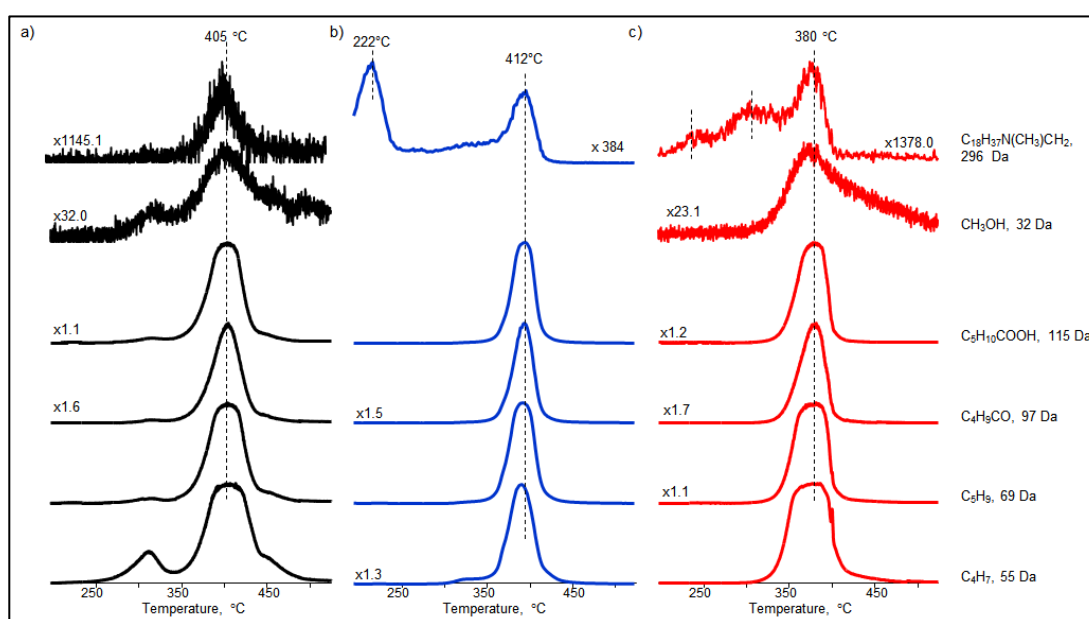
Figure 3. 32. Single ion evolution profiles of characteristic products detected during the pyrolysis of a) PCL, b) PCL-C15A and c) PCL-C30B

TIC curves and the pyrolysis mass spectra of BDBA recorded at the maximum of the TIC curves were given in Figure 3.33.

58
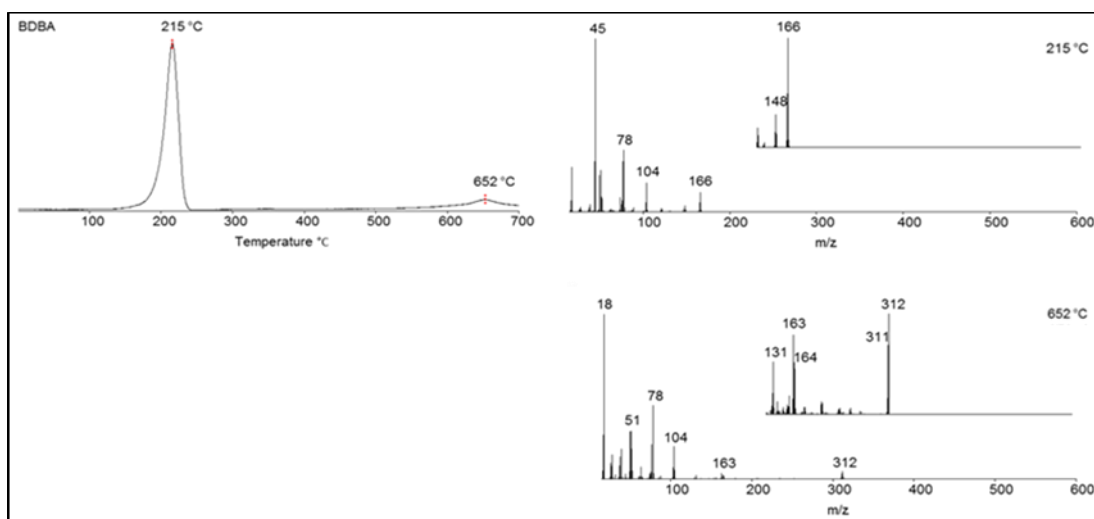
Figure 3. 33. Total ion current curve and mass spectra of BDBA at the peak maxima

The pyrolysis mass spectra of BDBA recorded at the maximum of the peaks at around 215°C showed the base peak at 45 Da assigned to $B(OH)_2$ fragment ion and the molecular ion peak of BDBA at 166 Da. Other peaks at 78 and 104 Da were associated with C_6H_6 and OBC_6H_4B, respectively. Additionally, the peak at 312 Da immerged at around 652°C was assigned to $(C_6H_5)_3CH_2B_3O_3$.

The TIC curves of PCL-BDBA composites involving various amounts of BDBA are given in Figure 3.34. The pyrolysis mass spectra recorded at the maximum of the peaks present in the TIC curves are also included in the figure.
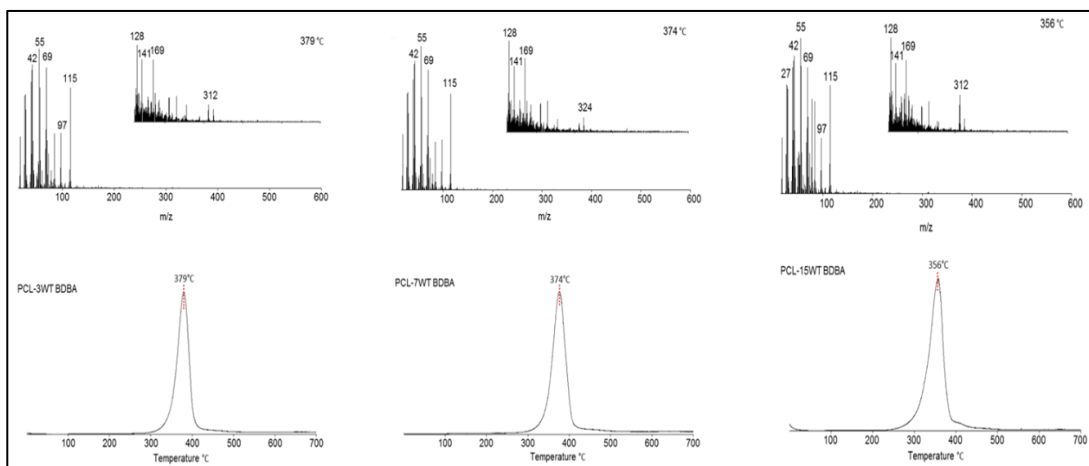
Figure 3. 34. Total ion current curve and mass spectra of PCL-3WT BDBA, PCL-7WT BDBA, PCL-15WT BDBA at the peak maxima

Thermal degradation temperatures for BDBA involving PCL composites were 379, 374 and 356°C with increasing BDBA content, respectively. When the amount of BDBA was increased, the thermal stability was decreased. For PCL-15WT BDBA composite, this decrease was pronounced, almost 20°C. The pyrolysis mass spectra recorded at peak maxima were very similar for all the composites under investigation. The base peak at 55 Da was assigned to C_3H_2OH. Other peaks at 69, 97 and 115 Da were associated with C_4H_4OH, C_6H_8OH and $C_5H_{10}COOH$, respectively.

In Figure 3.35, the TIC curves and the pyrolysis mass spectra recorded at the maximum of the peaks present in the TIC curves of PCL-C30B-BDBA composites involving various amounts of BDBA are given.

60
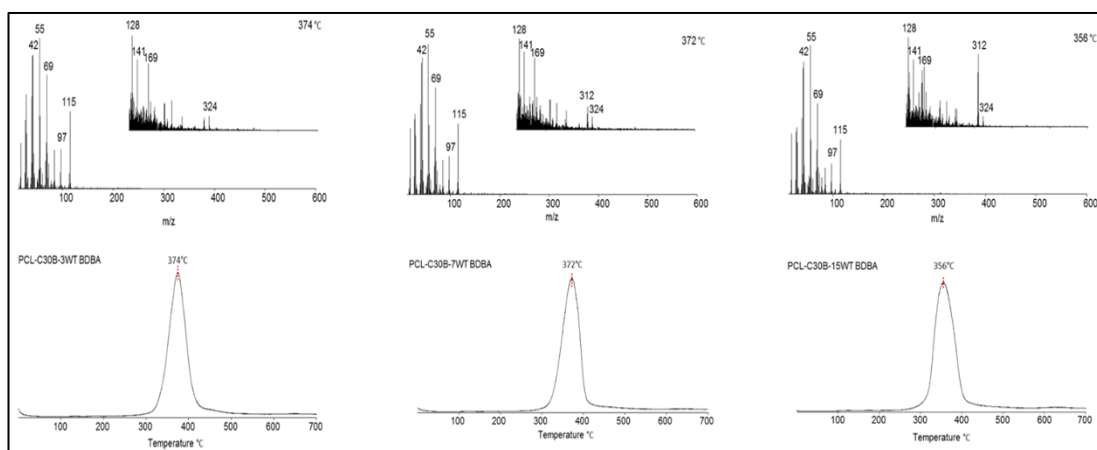
Figure 3. 35. Total ion current curve and mass spectrum of PCL-3WT C30B- 3WT BDBA, PCL-3WT C30B-7WT BDBA, PCL-3WT C30B-15WT BDBA at the peak maxima

Addition of C30B did not generate almost any change in temperature regions of thermal degradation and the pyrolysis mass spectra. The peak at 312 Da, associated with $(C_6H_5)_3(CH_2)B_3O_3$ was more significant when BDBA amount increased as expected.

Single ion evolution profiles of selected fragments of neat PCL and C30B and BDBA involving composites are presented in Figure 3.36.
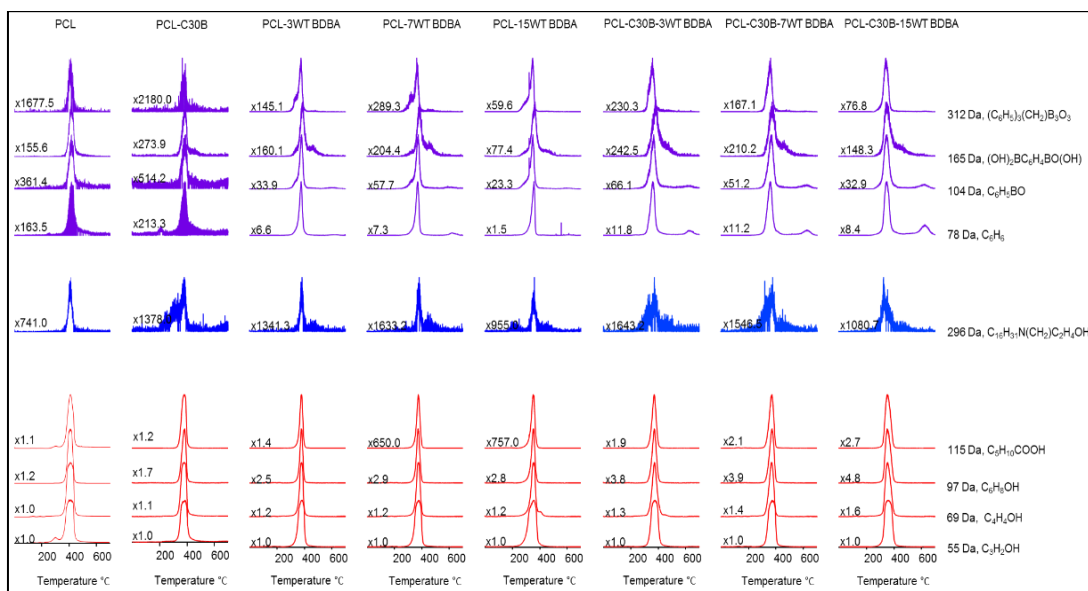
Figure 3. 36. Single ion evolution profiles of selected of neat PCL and C30B and BDBA involving composites

In the presence of nanoclay and boron compound, the low temperature peak in the TIC curve of PCL was disappeared, most probably due to the solution mixing process. A remarkable decrease in thermal stability of PCL-BDBA and PCL-C30B-BDBA was detected. Yet, the pyrolysis mass spectra of PCL and its composites were quite similar. Only small variations in the relative intensities of low mass fragments were detected.

TIC curves and the pyrolysis mass spectra recorded at the maximum of the peaks present in the TIC curves of PCL-C15A-BDBA composites involving various BDBA content are given in Figure 3.37.
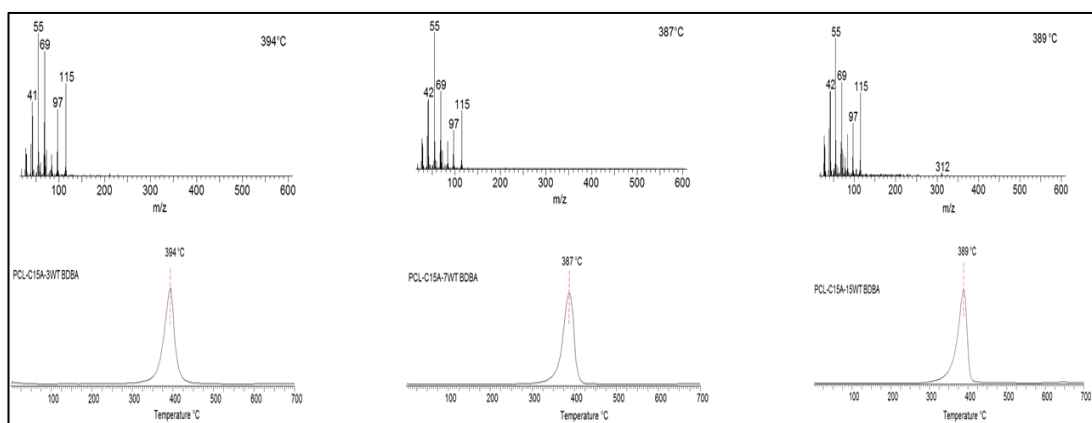
Figure 3. 37. Total ion current curve and recorded mass spectrum of PCL-C15A-3WT BDBA, PCL-C15A-7WT BDBA, PCL-C15A-15WT BDBA at the peak maxima

Thermal degradation of 3, 7 and 15 wt% C15A involving PCL-BDBA composites occurred at around 394, 387 and 389°C respectively. When the amount of BDBA was increased, the thermal stability was again decreased. The pyrolysis mass spectra recorded at peak maxima were very similar for all PCL composites. Addition of C15A instead of C30B did not generate any change in temperature regions for thermal degradation and pyrolysis mass spectra.

Upon incorporation of BDBA and/or C30B, the thermal stability of PCL was decreased. The decrease in thermal stability of PCL may be attributed to lower probability of crosslinking in the presence of long alkyl chains along the polymer backbone. Generation of boron network structure was detected for PCL-BDBA composites as shown in Scheme 1.
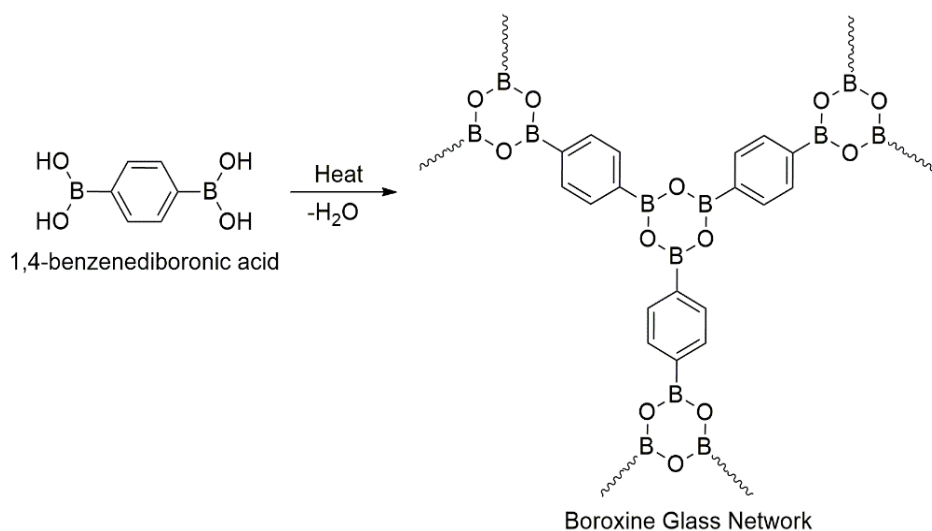
Scheme 1. Generation of boroxine glass network by removal of water from BDBA

For PCL, C30B, C15A and BDBA caused a decrease in thermal stability but extend of boron network at around 650°C was increased in the presence of clay. Trans-esterification reactions between BDBA and C30B and ester group of PCL were determined. The reaction mechanisms were shown in Scheme 2.
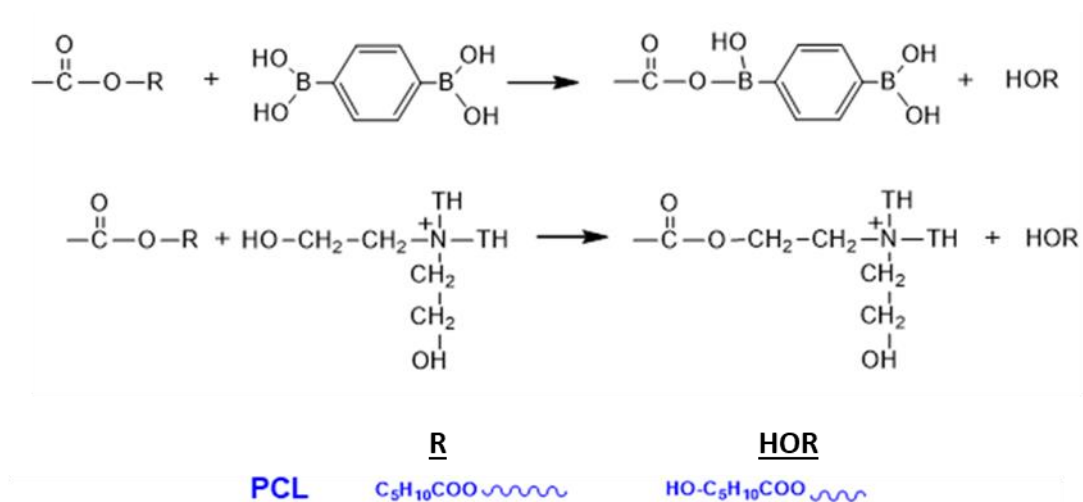
Scheme 2. Trans-esterification reactions BDBA and C30B with PCL

3.2.2.2.1 Gap Analysis of Decomposition Temperatures of PCL and Its C30B and BDBA Involving Composites

Thermal characteristics of PCL and its C30B and BDBA involving composites were studied by both DPMS and TGA analyses and results are summarized in Table 3. 7.

Table 3. 7 T_{dec} obtained by DPMS and TGA of neat PCL, PCL-C30B, PCL-C30B composites with 3, 7 and 15wt% BDBA

	T_{dec} from DPMS	T_{dec} from TGA
PCL	407	404
PCL-C30B	379	404
PCL-C30B-3wt BDBA	374	391
PCL-C30B-7wt BDBA	372	382
PCL-C30B-15wt BDBA	356	376

Decomposition temperatures of neat PCL determined by both techniques are very close to each other. However, when C30B and BDBA were added, significant differences between decomposition temperatures of composites was noted.

Gap analysis of decomposition temperatures of PCL and its C30B and BDBA involving composites are given in Figure 3.38.

Figure 3. 38. Gap analysis of decomposition temperatures of PCL and its C30B and BDBA involving composites

Although the decomposition temperatures of the composites obtained by these techniques showed variations, yet in general a decrease was observed. This divergence may be caused by the differences of characterization principles and sampling routes. For DPMS analyses, 2 µL sample solutions were poured into glass vials and after solvent evaporation, samples were heated up. On the other hand, for TGA analyses, solutions were poured onto Teflon surfaces and waited until all solvent was evaporated and samples were obtained as thin solid films. Therefore, especially for the samples involving additives the films may not be homogeneous.

3.2.2.2.2 Gap Analysis of Decomposition Temperatures of PCL and Its C15A and BDBA Involving Composites

Thermal decomposition of PCL and its C15A and BDBA involving composites obtained by both DPMS and TGA analyses are compared in Table 3. 8.

66

Table 3. 8 T_{dec} obtained by DPMS and TGA of neat PCL, PCL-C15A, PCL-C15A composites with 3, 7 and 15wt% BDBA

	T_{dec} from DPMS	T_{dec} from TGA
PCL	407	404
PCL-C15A	411	395
PCL-C15A-3wt BDBA	394	385
PCL-C15A-7wt BDBA	387	382
PCL-C15A-15wt BDBA	389	377

Decomposition temperatures determined by both techniques of neat PCL are very close to each other. However, when C15A and BDBA were added, the differences between decomposition temperatures of composites were detected.

Gap analysis of decomposition temperatures of PCL and its C15A and BDBA involving composites are given in Figure 3.39.
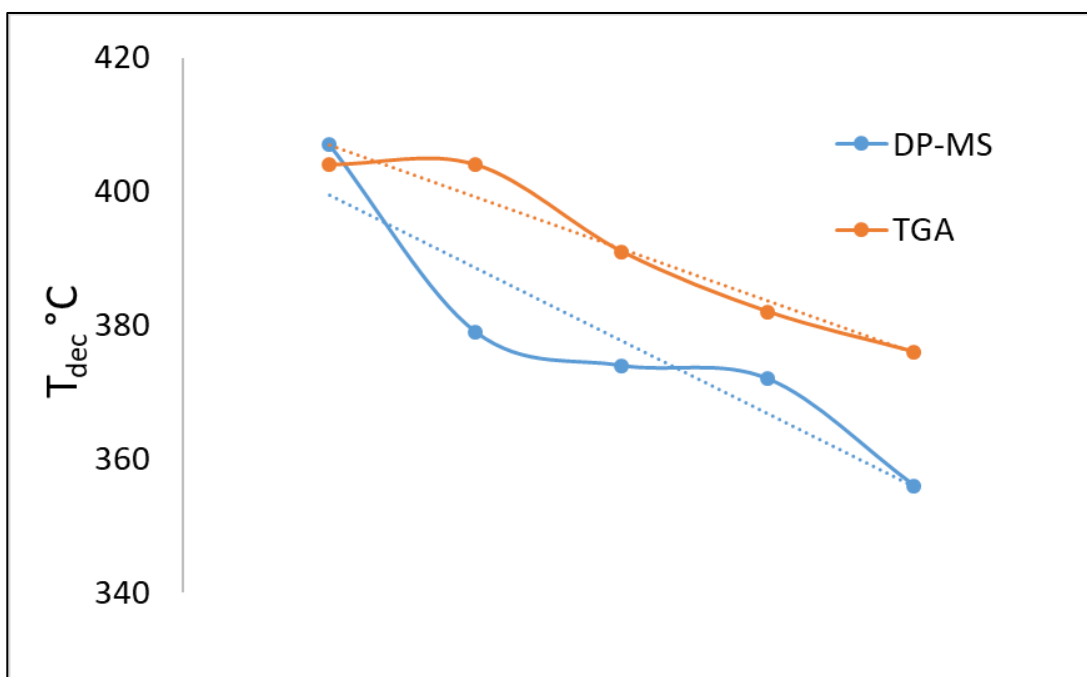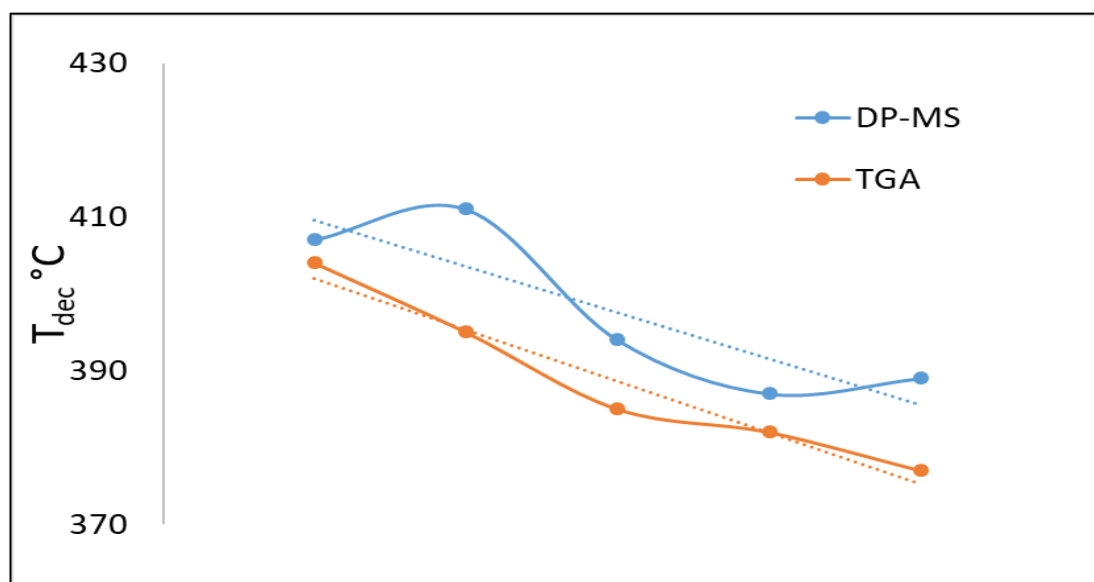

Figure 3. 39. Gap analysis of decomposition temperatures of PCL and its C15A and BDBA involving composites

Although the differences between the decomposition temperatures of composites obtained two techniques was detected compared to the neat PCL, a similar trend was again observed. This divergence may be explained by the differences of characterization principles and sampling routes. Sampling taken from the films may be nonhomogeneous especially for the additive involving samples for the TGA analyses.

3.2.2.3   PLA and Its Composites

TIC curves, the pyrolysis mass spectra at the maximum present in the TIC curves of PLA and PLA-C30B are given in Figure 3.40.

Figure 3.40. Total ion current curve and recorded mass spectrum of PLA and PLA-C30B at the peak maxima

The thermal degradation of neat PLA and PLA-C30B occurred at around 384 and 392°C, respectively. Thermal stability of PLA slightly shifted to the higher

temperature regions when C30B was introduced. The pyrolysis mass spectra recorded 384 and 392°C were quite similar. The peak at 45 Da and 56 Da were assigned to CO_2H and C_2H_4CO fragment ions, respectively.

The TIC curves of PCL-BDBA composites involving various amounts of BDBA are given in Figure 3.41. The pyrolysis mass spectra recorded at the maximum of the peaks present in the TIC curves are also presented in the figure.

Figure 3. 41. Total ion current curve and recorded mass spectrum of PLA-3wt BDBA, PLA-7wt BDBA and PLA-15wt BDBA at the peak maxima

Thermal degradation of BDBA involving PLA composites shifted to 378, 390 and 370°C in the presence of 3, 7 and 15 wt% BDBA respectively. Amount BDBA had no additional effect. The pyrolysis mass spectra recorded at peak maxima were very similar for all the samples, only relative intensities of the peaks were changed.

In Figure 3.42, TIC curves of PLA-C30B-BDBA composites involving various amounts of BDBA are given.

Figure 3. 42. Total ion current curve and recorded mass spectrum of PLA-C30B-3wt BDBA, PLA- C30B-7wt BDBA and PLA- C30B-15wt BDBA at the peak maxima

Thermal degradation of C30B involving PLA-BDBA composites were recorded at around 378, 378 and 383°C for 3, 7 and 15wt% BDBA involving composites respectively. Thermal stabilities of all PLA-C30B-BDBA composites were lower than that of PLA composite involving only C30B. The pyrolysis mass spectra recorded at peak maxima were very similar, again. The most intense peaks were at 28, 43 and 56 Da. The peat at 104 Da was again attributed to C_6H_5BO fragment ion.

Single ion evolution profiles of selected fragments of neat PLA and C30B and BDBA involving composites are presented in Figure 3.43.
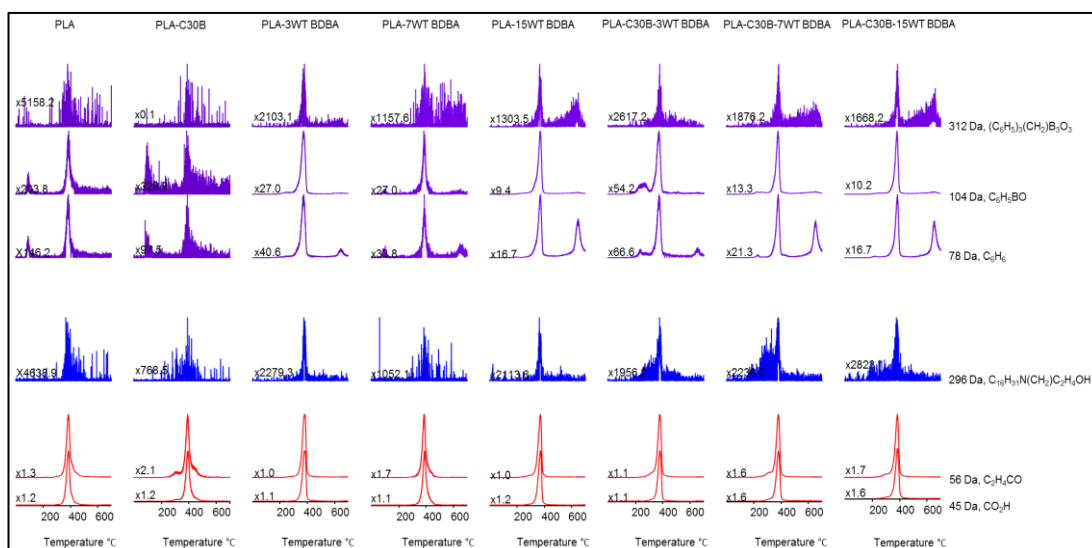
Figure 3. 43. Single ion evolution profiles of selected fragments of PLA, PLA-C30B, PLA-BDBA and PLA-C30B-BDBA composites

In Figure 3.43, single ion pyrograms of the degradation products of PLA and C30B and BDBA involving composites were depicted. The loss of low mass fragments, i.e. 45 and 56 Da was recorded at around 380°C. The slight increase in thermal stability with C30B addition became ineffective in the presence of BDBA. The weak peak around 650°C became more pronounced with increasing BDBA content.

Upon incorporation of BDBA and/or C30B, the thermal stability of PLA was increased. The increase in thermal stability of PLA can be associated with generation of a crosslinked structure, yet no boron network structure was detected due to temperature limitations. Products indicating trans-esterification reactions between BDBA and C30B and PLA were determined. The reaction mechanisms are shown in Scheme 3.
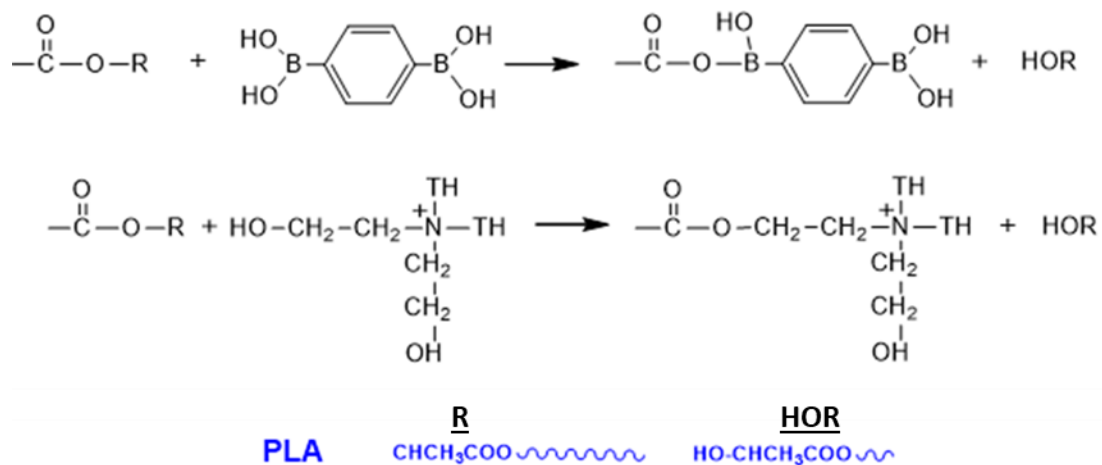
Scheme 3. Trans-esterification reactions BDBA and C30B with ester groups of PLA

3.2.2.4   PMMA and Its Composites

The TIC curves of PMMA and PMMA-C30B composites are given in Figure 3.44. The pyrolysis mass spectra recorded at the maximum of the peaks present in the TIC curves are also included in the figure.
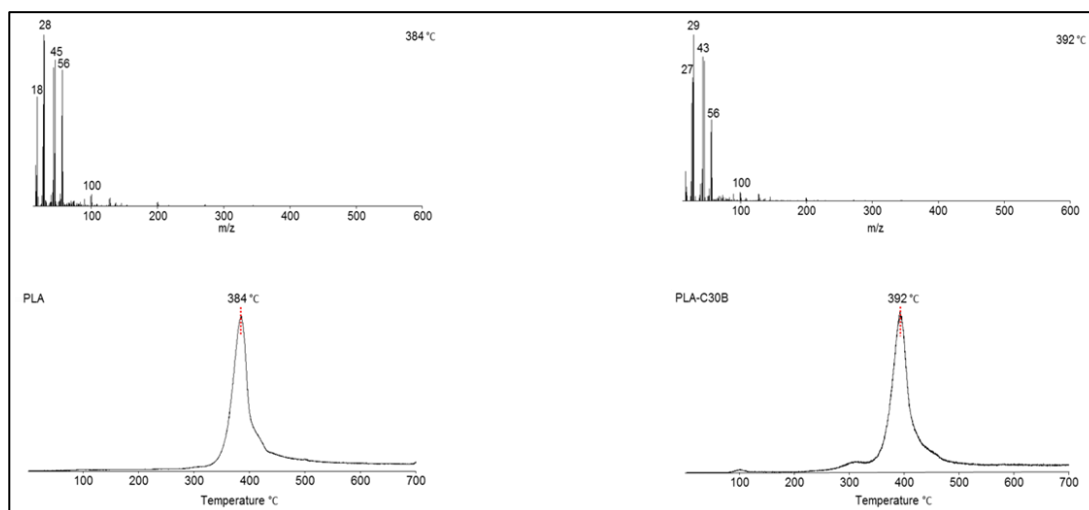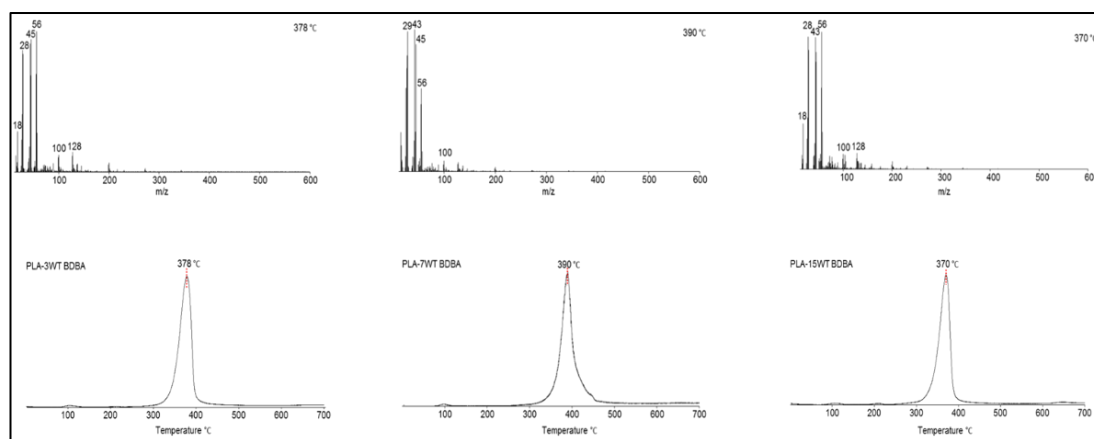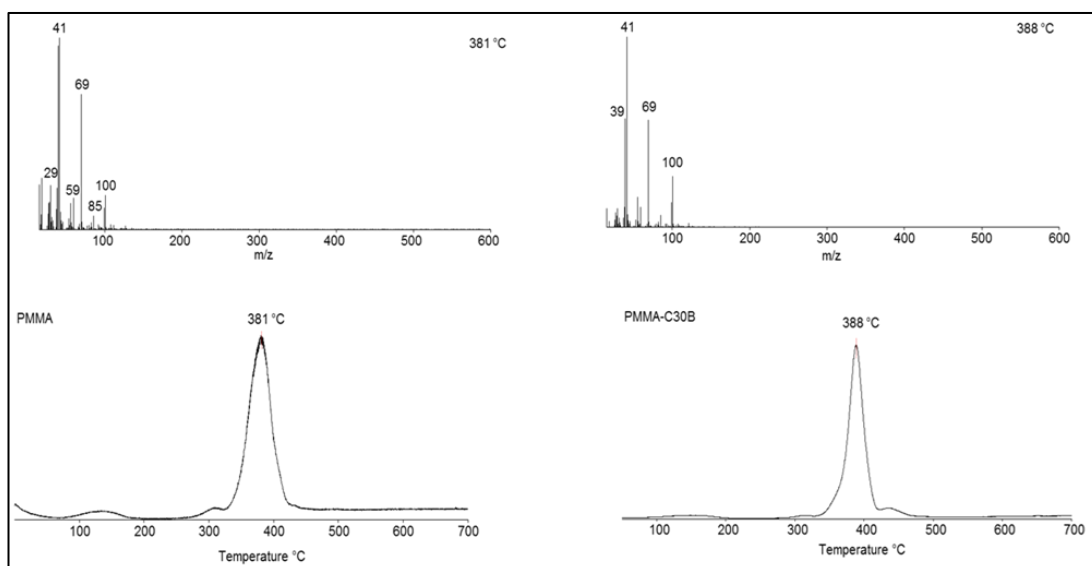
Figure 3. 44. Total ion current curve and mass spectrum of PMMA and PMMA-C30B at the peak maxima

The thermal degradation of neat PMMA and PMMA-C30B mainly occurred at around 381 and 388°C, respectively. Thermal stability of PMMA slightly shifted to the higher temperatures when C30B was introduced. The pyrolysis mass spectra recorded at peak maxima were quite similar. The base peak was at 41 Da assigned to C_3H_5 fragment ion. Other intense peaks at 69 and 100 Da were associated with C_3H_5CO and methyl methacrylate monomer, respectively.

The TIC curves and the pyrolysis mass spectra recorded at the maximum of the peaks of PMMA-BDBA composites involving various amounts of BDBA are presented in Figure 3.45.
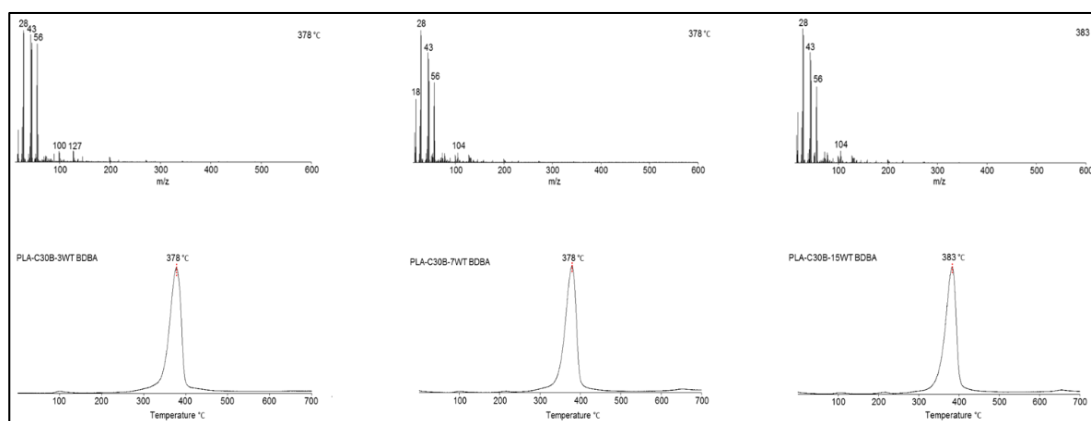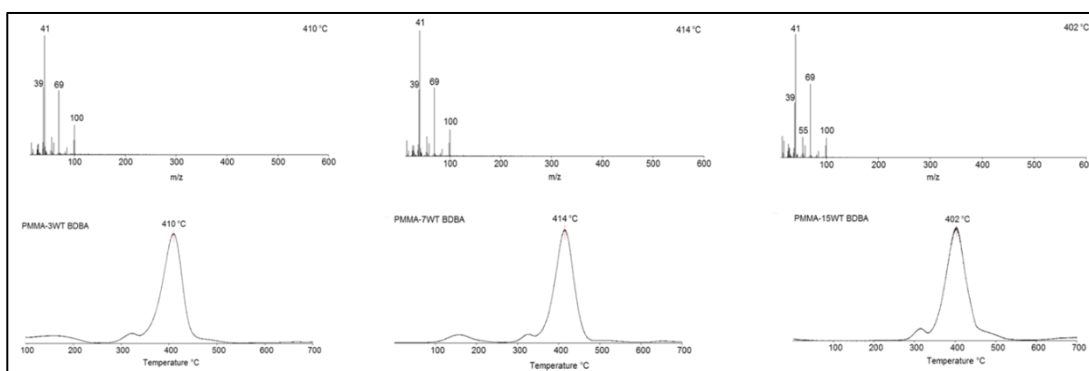
Figure 3. 45. Total ion current curve and mass spectrum of PMMA-3wt BDBA, PMMA-7wt BDBA and PMMA-15wt BDBA at the peak maxima

Thermal degradation of 3, 7 and 15 wt% BDBA involving PMMA composites took place at around 410, 414 and 402°C respectively. Thermal stability of PMMA was increased when BDBA was added compared to neat PMMA and PMMA-C30B composite. The pyrolysis mass Spectra recorded at peak maxima were almost the same for all PMMA-BDBA composites.

TIC curves of PMMA-C30B-BDBA composites involving various amount of BDBA are given in Figure 3.46.

Figure 3. 46. Total ion current curve and recorded mass spectrum of PMMA-C30B-3wt BDBA, PMMA- C30B-7wt BDBA and PMMA- C30B-15wt BDBA at the peak maxima

Thermal degradation of C30B involving PMMA composites involving 3, 7 and 15wt% BDBA took around 405, 411 and 415°C, respectively. Thermal stabilities of all PMMA-C30B-BDBA composites were higher than neat PMMA and PMMA-C30B composite. The pyrolysis mass spectra recorded at peak maxima were again very similar. The base peak was at 41 Da. The other intense peaks were at 69 and 100 Da.

Single ion evolution profiles of selected fragments of neat PMMA and C30B and BDBA involving composites are presented in Figure 3.47.
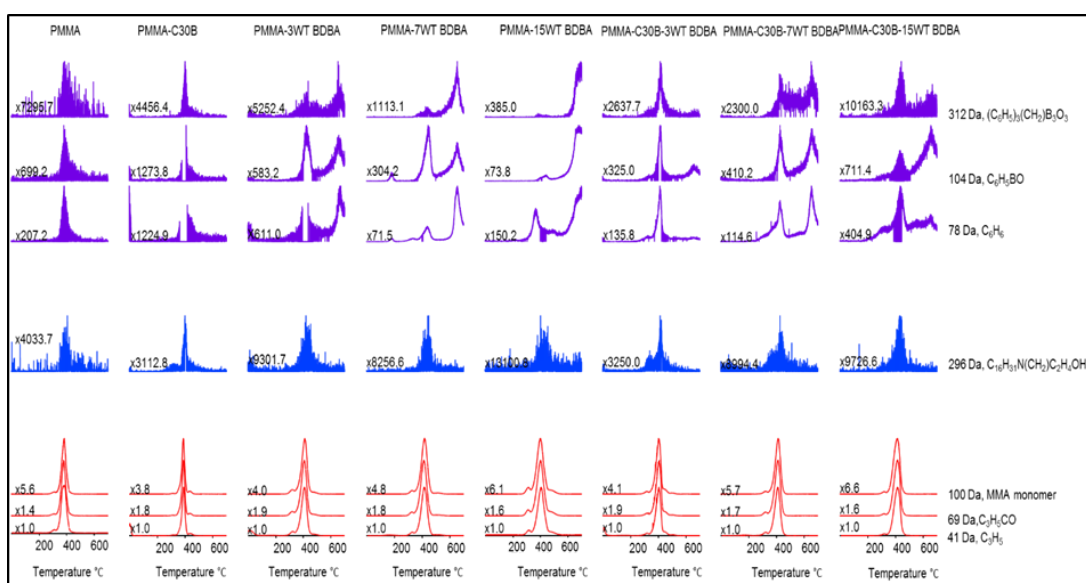
Figure 3. 47. Single ion evolution profiles of selected fragments of PMMA, PMMA-C30B, PMMA-BDBA and PMMA-C30B-BDBA composites

Single ion pyrograms of the degradation products of PLA and C30B and BDBA involving composites were depicted in Figure 3.45. The peaks at 78, 104 and 312 Da were assigned to C_6H_6, C_6H_5BO and $(C_6H_5)_3(CH_2)B_3O_3$, respectively. The peak

intensities and decomposition temperatures showed differences as the amount of BDBA was increased.

Upon incorporation of BDBA and/or C30B, the thermal stability of PMMA was increased. The increase in thermal stabilities of PMMA can be associated with generation of a crosslinked structure. Moreover, generation of boron network structure was detected for PMMA-BDBA composites. For PMMA, extent of boron network was decreased in the presence of clay. Products that may be generated by trans-esterification reactions between BDBA and C30B and ester groups of PMMA were determined. The reaction mechanisms are shown in Scheme 4.
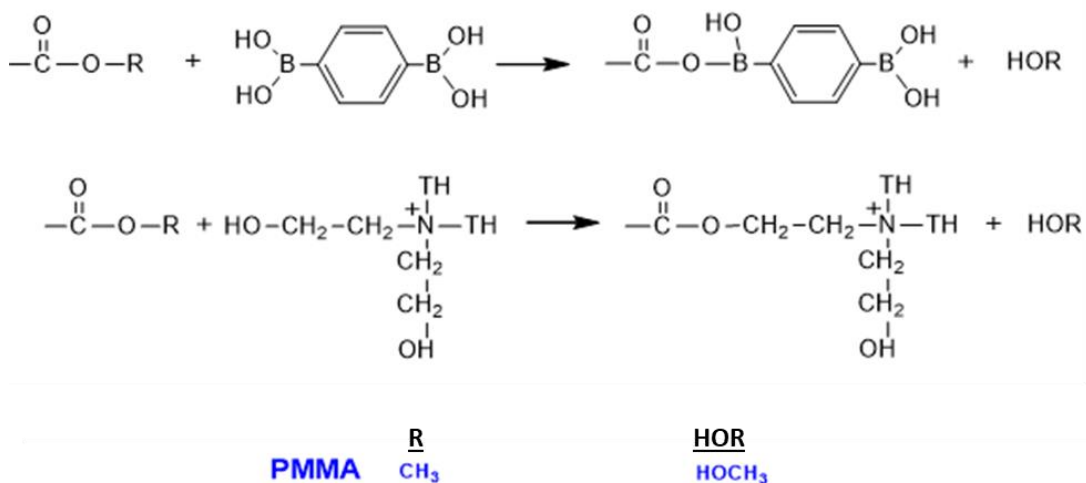
Scheme 4. Trans-esterification reactions BDBA and C30B with ester groups of PMMA

3.2.2.5   PNBMA and Its Composites

In Figure 3.48, TIC curves and pyrolysis mass spectra recorded at the maximum of the peaks present in the TIC curves of PNBMA and PNBMA-C30B composites are given.
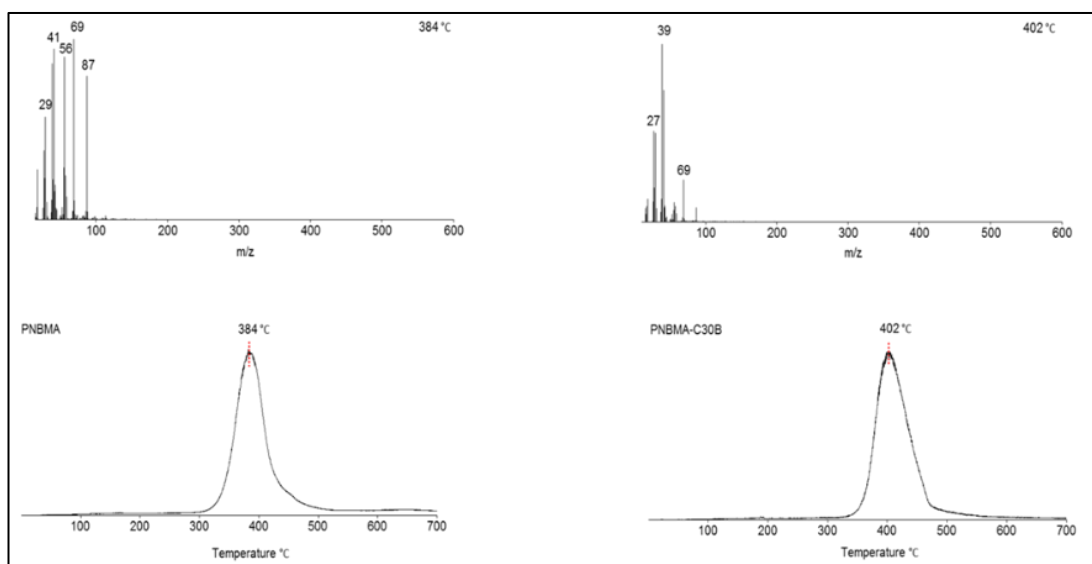
Figure 3. 48. Total ion current curve and recorded mass spectrum of PNBMA and PNBMA-C30B at the peak maxima

The thermal degradation of neat PNBMA was maximized at around 384°C and when C30B was introduced, it shifted about 20°C to higher temperatures. The pyrolysis mass spectra at peak maxima were quite different. The base peak was at 69 Da which was assigned to C_3H_5CO fragment ion for neat PNBMA. The other intense peaks were recorded at 41 and 87 Da were associated with C_3H_5 and $C_3H_5(OH)_2$, respectively. On the other hand, the base peak for PNBMA-C30B composite was at 39 Da.

The TIC curves and the pyrolysis mass spectra recorded at the maximum of the peaks present in the TIC curves of PNBMA-BDBA composites involving various amounts of BDBA are presented in Figure 3.49.
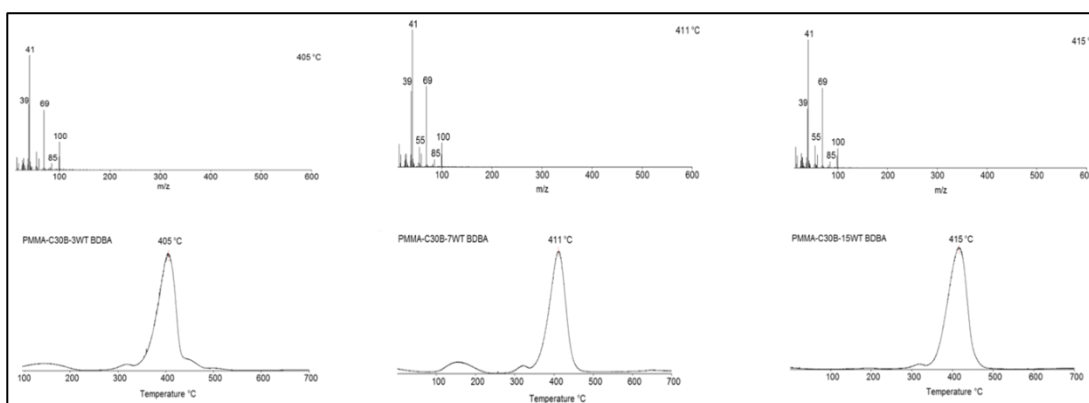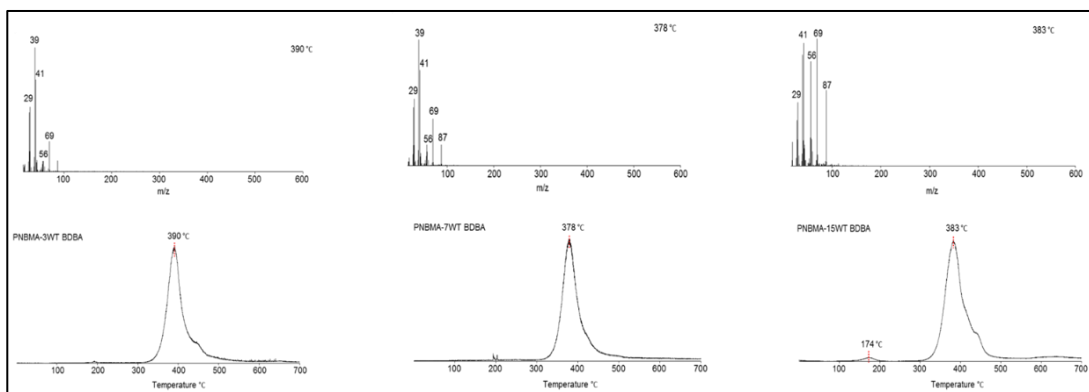
Figure 3. 49. Total ion current curve and recorded mass spectrum of PNBMA-3wt BDBA, PNBMA-7wt BDBA and PNBMA-15wt BDBA at the peak maxima

Thermal degradation of BDBA involving PNBMA composites involving 3, 7 and 15 wt % BDBA took place at around 390, 378 and 483°C respectively. Thermal stability of the PNBMA composites was not directly proportional with BDBA amount. Thermal stability of PNBMA was decreased when BDBA was added compared to PNBMA-C30B composite. A weak peak occurred at around 174°C for PNBMA-15wt BDBA. The pyrolysis mass spectra recorded at peak maxima were quite similar, only some changes in the relative intensities of the peaks were detected. TIC curves of PNBMA-C30B-BDBA composites involving various amount of BDBA are given in Figure 3.50.
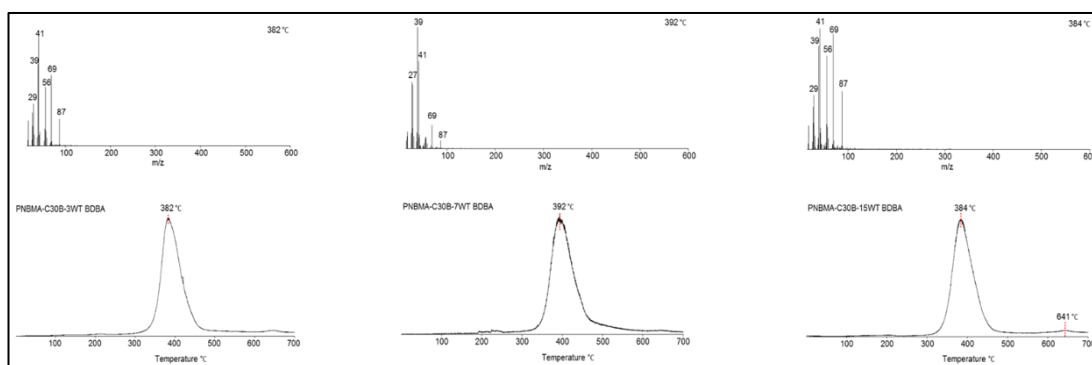
Figure 3. 50. Total ion current curve and the mass spectrum at the peak maximum of the TIC curve of PNBMA-C30B-3wt BDBA, PNBMA- C30B-7wt BDBA and PNBMA- C30B-15wt BDBA

Thermal degradation of C30B involving 3, 7 and 15 wt% PNBMA-BDBA composites were 382, 392 and 384°C, respectively. Thermal stabilities of all PNBMA-C30B-BDBA composites were lower than that of PNBMA-C30B composite. The pyrolysis mass Spectra recorded at peak maxima were again very similar. There was another weak peak at around 650°C for PNBMA-C30B-BDBA composites.

Single ion evolution profiles of selected fragments of neat PNBMA and C30B and BDBA involving composites are presented in Figure 3.51.
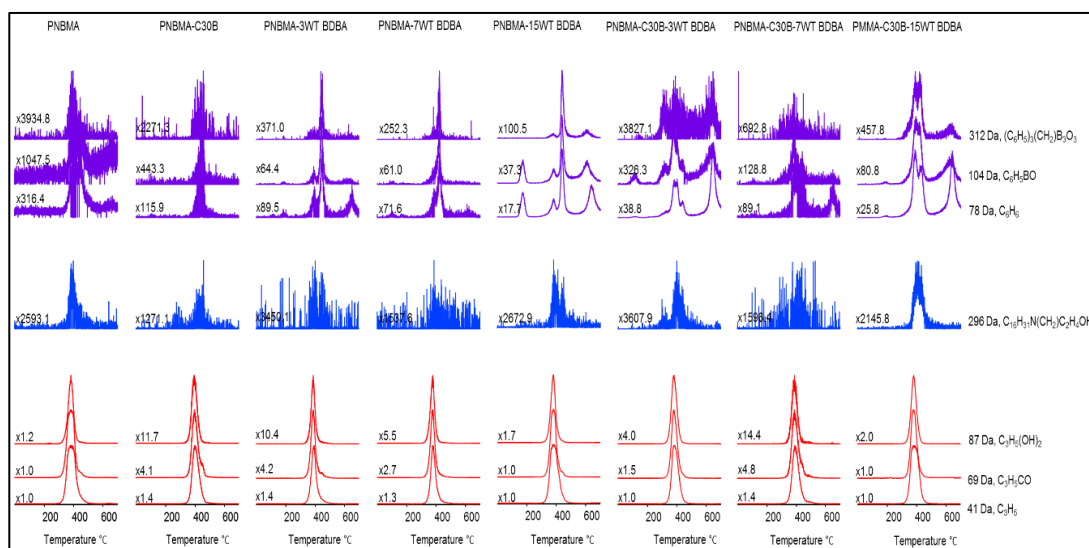
Figure 3. 51. Single ion evolution profiles of selected fragments of PNBMA, PNBMA-C30B, PNBMA-BDBA and PNBMA-C30B-BDBA composites

In Figure 3.51, single ion pyrograms of the degradation products of PNBMA and C30B and BDBA involving composites were depicted. No remarkable change in thermal stability of PNBMA-BDBA and PNBMA-C30B-BDBA was detected. In addition, the pyrolysis mass spectra of PNBMA and its composites were quite similar. Only small variations in relative intensities of low mass fragments were detected.

For PnBMA, although addition of C30B increased the thermal stability of polymer, addition of BDBA caused no noticeable change in thermal stability. However, BDBA-polymer interaction was increased in the presence of clay.

CHAPTER 4

CONCLUSION

In the first part of this study, morphological characteristics of polyesters and their composites involving various amounts of clay and boron compounds were determined. Disappearance of the clay peaks can be considered as both dispersion of clay structures in the polymer matrices and the well separation of the tactoid structure of clays. In order to support this inference, TEM images of polyester-clay-boron composites were obtained and both intercalated and partially exfoliated clay layers exist.

Electrospun fibers of PCL and its composites were prepared and characterized. DCM-DMF solvent system with 80:20 (v/v) solvent ratio and 15wt% PCL concentration were chosen as the most suitable conditions in order to obtain relatively better PCL fibers.

In the second part, thermal characteristics of polyesters and their clay and boron involving composites were investigated by TGA, DTG and DPMS.

Upon incorporation of BDBA and/or C30B, the thermal stabilities of PLA and PMMA were increased whereas that of PCL was decreased. The increase in thermal stabilities of PLA and PMMA can be associated with generation of a crosslinked structure. On the other hand, the decrease in thermal stability of PCL may be attributed to lower probability of crosslinking in the presence of long alkyl chains along the polymer backbone. Generation of boron network structure was detected for PMMA-BDBA and PCL-BDBA composites.

For PMMA, extent of boron network was decreased in the presence of clay. Addition of clay increased the thermal stability of PLA whereas no boron network structure was detected due to temperature limitations. For PCL, C30B, C15A and BDBA caused a decrease in thermal stability but contrary to PMMA, extend of boron

network at around 650°C was increased in the presence of clay. For PnBMA, although C30B increased the thermal stability, addition of clay with BDBA caused any noticeable change in thermal stability. However, BDBA-polymer interaction was increased in the presence of clay. Trans-esterification reactions between BDBA and C30B and ester groups of polymer matrices were determined.

REFERENCES

[1] Wang, G., Yu, D., Kelkar, A. and Zhang, L. 2017. Electrospun nanofiber: emerging reinforcing filler in polymer matrix composite materials, Progress in Polymer Science, 75, doi: 10.1016/j.progpolymsci.2017.08.002.

[2] Pahlevanzadeh, F., Bakhsheshi-Rad, H. Y., Brabazon, D., Kharaziha, M., Ismail, A. F., Sharif, S., Razzaghi, M. and Berto, F., 2021. Additive Manufacturing of Polymer Matrix Composites, Reference Module in Materials Science and Materials Engineering, Elsevier.

[3] Mhaske, S. T. and Gadgeel, A., 2021. Multi-Functional Polymer-Matrix Composites, Reference Module in Materials Science and Materials Engineering, Elsevier.

[4] Zou, H., Shishan, W. and Shen, J. 2008. Polymer/silica nanocomposites: preparation, characterization, properties and applications, Chemical Reviews, 108. 3893-3957.

[5] Tjong, S. C. 2006. Structural and mechanical properties of polymer nanocomposites, Materialas Science and Engineering: Reports, 53. 73-197.

[6] Kwon, N. K., Kim, H., Han, I. K., Shin, T. J., Lee, H. W., Park, J. and Kim, S. Y. 2018. Enhanced mechanical properties of polymer nanocomposites using dopamine-modified polymers at nanoparticle surfaces in very low molecular weight polymers, ACS Macro Letters, 7. 962-967.

[7] Majka, T. M., Leszczynska, A. and Pielichowski, K. 2016. Thermal stability and degradation of polymer nanocomposites, Polymer Nanocomposites, 167-190.

[8] Carvalho, H. W. P., Santilli, C. V., Briois, V. and Pulcinelli, S. 2013. Polymer-clay nanocomposites thermal stability: experimental evidence of the radical trapping effect, RSC Advances, 3. 22830-22833.

[9] Cui, Y., Kumar, S., Kona, B. R. and Houcke, D. 2015. Gas barrier properties of polymer/clay nanocomposites, RSC Advances, 5. 63669-63690.

[10] Fang, F. F., Choi, H. J. and Joo, J. 2008. Conducting polymer/clay nanocomposites and their applications, Journal of Nanoscience and Nanotechnology, 8. 1559-1581.

[11] Kumar, S. and Maiti, P. 2016. Controlled biodegradation of polymers using nanoparticles and its application, RSC Advances, 6. 67449-67480.

[12] Armentano, I., Puglia, D., Luzi, F., Arciola, C. R., Morena, F., Martino, S. and Torre, L. 2018. Nanocomposites based on biodegradable polymers, Materials (Basel), 11 (5), 795.

[13] Lu, Y. L., Wu, Y. P. and Zhang, L. Q. 2009. Processing of macro, micro and nanocomposites, Advances in Polymer Processing, 479-551.

[14] Akar, A. O. and Hacaloglu, J. 2020. Preparation and characterization of poly(lactic acid) composites involving aromatic diboronic acid and organically modified montmorillonite, Journal of Thermal Analysis and Calorimetry, doi: https://doi.org/10.1007/s10973-019-09236-y.

[15] Goktas, M. and Hacaloglu, J. 2019. Poly(methyl methacrylate) nanocomposites involving aromatic diboronic acid, Polymer Bulletin, 76. 6231-6243.

[16] Cesur, S., Köroğlu, C. and Yalçın, H. T. 2017. Antimicrobial and biodegradable food packaging applications of polycaprolactone/organo nanoclay/chitosan polymeric composite films, Journal of Vinyl and Additive Technology, 24. 376-387.

[17] Karuppuswamy, P., Venugopal, J. R., Navaneethan, B., Laiva, A. L. and Ramakrishna, S. 2015. Polycaprolactone nanofibers for the controlled release of tetracycline hydrochloride, Materials Letters, 141. 180-186.

[18] Abudula, T., Gauthaman, K., Mostafavi, A., Alshahrie, A., Salah, N., Morganti, P., Chianese, A., Tamayol, A. and Memic, A. 2020. Sustainable drug release from polycaprolactone coated chitin-lignin gel fibrous scaffolds, Scientific Reports, 10. 20428.

[19] Siddiqui, N., Asawa, S., Birru, B., Baadhe, R. and Rao, S. 2018. PCL-based composite scaffold matrices for tissue engineering applications, Molecular Biotechnology, 60. 506-532.

[20] Ahmed, J., Auras, R., Kijchavengkul, T. and Varshney, S. K. 2012. Rhelogical, thermal and structural behavior of poly(ε-caprolactone) and nanoclay blended films, Journal of Food Engineering, 111. 580-589.

[21] Moussaif, N., Crespo, C., Meier, J. G. and Jimenez, M. A. 2012. Synergistic reinforcement of nanoclay and mesoporous silicate fillers in polycaprolactone: the effect of nanoclay on the compatibility of the components, Polymer, 53. 3741-3748.

[22] Yahiaoui, F., Benhacine, F., Harrar, H. F., Habi, A., Hamou, A. S. and Grohens, Y. 2015. Development of antimicrobial PCL/nanoclay nanocomposite films with enhanced mechanical and water vapor barrier properties for packaging applications, Polymer Bulletin, 72. 235-254.

[23] Chen, B. Y., Wang, Y. S., Mi, H. Y. and Yu, P. 2014. Effect of poly(ethylene glycol) on the properties and foaming behavior of macroporous poly(lactic acid)/sodium chloride scaffold, Journal of Applied Polymer Science, 131. doi: 10.1002/app.41181.

[24] Keshtkar, M., Nofar, M., Park, C. B. and Carreau, P. J. 2014. Extruded PLA/clay nanocomposite foams blown with supercritical CO2, Polymer, 55. 4077-4090.

[25] Ali, U., Juhanni, K., Karim, A. and Buang, N. A. 2015. A review of the properties and applications of poly (methyl methacrylate)(PMMA), Polymer Reviews, 55. 678-705.

[26] Shah, R., Kausar, A., Muhammad, B. and Khan, M. 2016. Investigation on thermal conductivity and physical properties of polythiophene/p-phenylenediaminegraphene oxide and polythiophene-co-poly (methyl methacrylate)/p-phenylenediamine graphene oxide composites, Composite Interfaces, 23. 887-899.

[27] Shah, J. J., Geist, J., Locascio, L. E., Gaitan, M., Rao, M. V. and Vreeland, W. N. 2006. Surface modification of poly(methyl methacrylate) for improved adsorption of wall coating polymers for microchip electrophoresis, Electrophoresis, 27. 3788-3796.

[28] Costache, M. C., Wang, D., Heidecker, M. J., Manias, E. and Wilkie, C. A. 2006. The thermal degradation of poly(methyl methacrylate) nanocomposites with montmorillonite, layered double hydroxides and carbon nanotubes, Polymers for Advanced Technologies, 17. 272-280.

[29] Weightman, B., Freeman, M. A., Revel, P. A., Braden, M., Albrektsson, B. E. and Carlson, L. V. 1987. On the relationship between the mechanical properties of cement and loosening of total hip femoral components, The Journal of Bone and Joint Surgery, 69. 558-564.

[30] Hill D. J. T., Moss, N. G., Pomery, P. J. and Whittaker, A. K. 2000. Copolymer hydrogels of 2-hydroxyethyl methacrylate with *n*-butyl methacrylate and cyclohexyl methacrylate: synthesis, characterization and uptake of water, Polymer, 41. 1287-1296.

[31] Chen, J., Carrot, C., Chalamet, Y., Majeste, J. C. and Taha, M. 2003. Rheology of poly(*n*-butyl methacrylate) and its composites with calcium carbonate, Journal of Applied Polymer Science, 88. 1376-1383.

[32] Urbanczyk, L., Calberg, C., Stassin, F., Alexandre, M., Jerome, R., Jerome, C. and Detrembleur, C. 2008. Synthesis of PCL/clay masterbatches in supercritical carbon dioxide, Polymer, 49. 3979-3986.

[33] Singh, N. K., Purkayastha, B. D., Roy, J. K., Banik, R. M., Yashpal, M., Singh, G., Malik, S. and Maiti, P. 2010. Nanoparticle-Induced Controlled

Biodegradation and Its Mechanism in Poly(ε-caprolactone), ACS Applied Materials & Interfaces, 2. 69-81.

[34] Said, S., Eltaher, H. M. and Khordagui, L. K. 2019. Biomedical applications of composite resorbable fibers, Materials for Biomedical Engineering: Absorbable Polymers, 127-155.

[35] Frenot, A. and Chronakis, I. S. 2003. Polymer nanofibers assembled by electrospinning, Current Opinion in Colloid & Interface Science, 8. 64-75.

[36] Tan, S. H., Inai, R., Kotaki, M. and Ramakrishna, S. 2005. Systematic parameter study for ultra-fine fiber fabrication via electrospinning process, Polymer, 46. 6128-6134.

[37] He, J. H., Wan, Y. Q. and Yu, J. Y. 2005. Scaling law in electrospinning: relationship between electric current and solution flow rate, Polymer, 46. 2799-2801.

[38] Reneker, D. H. and Yarin, A. L. 2008. Electrospinning jets and polymer nanofibers, Polymer, 49. 2387-2425.

[39] Huang, Z. M., Zhang, Y., Kotaki, M. and Ramakrishna, S. 2003. A review on polymer nanofibers by electrospinning and their applications in nanocomposites, Composites Science and Technology, 63. 2223-2253.

[40] Lu, P. and Ding, B. 2008. Applications of electrospun fibers, Recent Patents on Nanotechnology, doi: 10.2174/187221008786369688.

[41] Touny, A. H. and Bhaduri, S. B. 2010. A reactive electrospinning approach for nanoporous PLA/monetite nanocomposite fibers, Materials Science and Engineering: C, 30. 1304-1312.

[42] Lin, J., Ding, B., Yu, J. and Hsieh, Y. 2010. Direct fabrication of highly nanoporous polystyrene fibers via electrospinning, ACS Applied Materials & Interfaces, 2. 521-528.

[43] Dalir, H., Farahani, R. D., Nhim, V., Samson, B., Levesque, M. and Therriault, D. 2021. Preparation of highly exfoliated polyester clay nanocomposites process property correlations, Langmuir, 28. 791-803.

[44] Bagheri, K., Razavi, S. M., Ahmadi, S. J., Kosari, M. and Abolghasemi, H. 2018. Thermal resistance, tensile properties, and gamma radiation shielding performance of unsaturated polyester/nanoclay/PbO composites, Radiation Physics and Chemistry, 146. 5-10.

[45] Romanzini, D., Frache, A., Zattera, A. J. and Amico, S. C. 2015. Effect of clay silylation on curing and mechanical and thermal properties of unsaturated polyester/montmorillonite nanocomposites, Journal of Physics and Chemistry of Solids, 87. 9-15.

[46] Chieruzzi, M., Miliozzi, A. and Kenny, J. M. 2013. Effects of the nanoparticles on the thermal expansion and mechanical properties of unsaturated polyester/clay nanocomposites, Compos. Part A, 45. 44-48.

[47] Lepoittevin, B., Devalckenaere, M., Pantoustier, N., Alexandre, M., Kubies, D., Calberg, C., Jerome, R. and Dubois, P. 2002. Poly(ε-caprolactone)/clay nanocomposites prepared by melt intercalation: mechanical, thermal and rheological properties, Polymer, 43. 4017-4023.

[48] Ozdemir, E. and Hacaloglu, J. 2017. Poly(methyl metacrylate) organoclay composites; interactions of organic modifier with the polymer effecting thermal degradation behavior, European Polymer Journal, 95. 474-481.

CURRICULUM VITAE

PERSONAL INFORMATION

Surname, Name: Çetinkaya, Nezaket Nehir
Nationality: Turkish (TC)
Date and Place of Birth: 1 September 1988, Ankara
Marital Status: Married
Phone: +90 536 067 98 81
email: e160647@metu.edu.tr

EDUCATION

Degree	Institution	Year of Graduation
MS	METU Polymer Science and Technology	2015
BS	METU Chemistry	2012
High School	Yıldırım Beyazıt Anatolian High School, Ankara	2006

WORK EXPERIENCE

Year	Place	Enrollment
2017-Present	TÜPRAŞ	Laboratory Chief
2011-2011	Ankara Forensic Science Foundation	Intern

FOREIGN LANGUAGES

Advanced English

PUBLICATIONS

IN PREPARATION

1. Utku N., Kaynak, C. and Hacaloğlu J. "The Effects of Boron Compounds on Thermal Degradation Behavior of Polymers Involving Ester Linkages"

2. Utku N., Kaynak, C. and Hacaloğlu J. "Preparation and Thermal Characterization of Polycaprolactone Electrospun Nanofibers"

SUBMITTED

1. Utku N. and Hacaloğlu J. "The Effects of Organically Modified Montmorillonite on Thermal Characteristics of Polylactic Acid and Polycaprolactone", Polymer Bulletin